

Speed: 3D sensors, current amplifiers

Cinzia Da Via

Manchester University

Giovanni Anelli, Matthieu Despeisse¹, Pierre Jarron

CERN

Christopher Kenney, Jasmine Hasi,

SLAC

Angela Kok

SINTEF

Sherwood Parker

University of Hawaii

Initial work and calculations with **Julie Segal**

Wall electrode data with **Edith Walckiers**, Philips Semiconductors AG

1. now at Ecole Polytechnique Fédérale de Lausanne (EPFL), Institute of Microengineering (IMT), Photovoltaics and thin film electronics laboratory, Neuchatel, Switzerland.

- 1. introduction**
- 2. history**
- 3. factors affecting speed**
- 4. generating the signal – Ramo's theorem**
- 5. amplifying the signal – charge and current amplifiers**
- 6. trench electrode sensors**
- 7. hex-cell sensors**
- 8. experimental results**
- 9. analysis – constant fraction discrimination**
- 10. analysis – fitting with almost-noise-free pulses**
- 11. next**

Keys to the technology

1. Plasma etchers can now make **deep, near-vertical holes and trenches:**

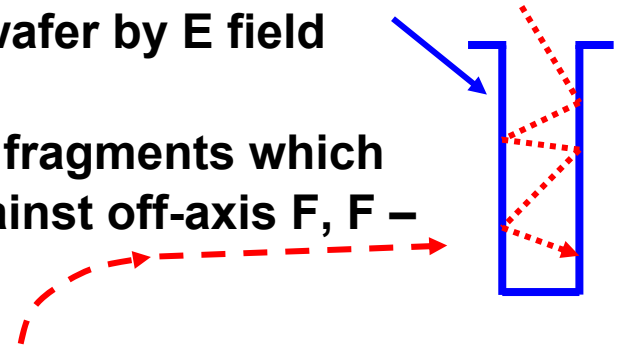
a. SF_6 in plasma \rightarrow F , F^- \rightarrow driven onto wafer by E field

b. $\text{Si} + 4\text{F} \rightarrow \text{SiF}_4$ (gas)

c. SF_6 replaced with $\text{C}_4\text{F}_8 \rightarrow \text{CF}_2$ + other fragments which

d. form teflon-like wall coat protecting against off-axis F , F^-

e. repeat (a – d) every 10 – 15 seconds



2. At $\sim 620^\circ\text{C}$, ~ 0.46 Torr, SiH_4 , SiH_2Cl_2 , SiHCl_3 , and / or SiCl_4 gas molecules bounce off the walls many times before they stick, mostly entering and leaving the hole. When they stick, it can be anywhere, so they form a conformal polysilicon coat as the H or Cl leaves and the silicon migrates to a lattice site.

3. Gasses such as B_2O_3 , B_2H_6 (diborane), P_2O_5 , and PH_3 (phosphine) can also be deposited in a conformal layer, and make p^+ and n^+ doped polysilicon.

4. Heating drives the dopants into the single crystal silicon, forming p-n junctions and ohmic contacts there. Large E drift fields can end before the poly, removing that source of large leakage currents.

5. Active edges are made from trench electrodes, capped with an oxide coat. Plasma dicing up to the oxide etch stop makes precise edges.

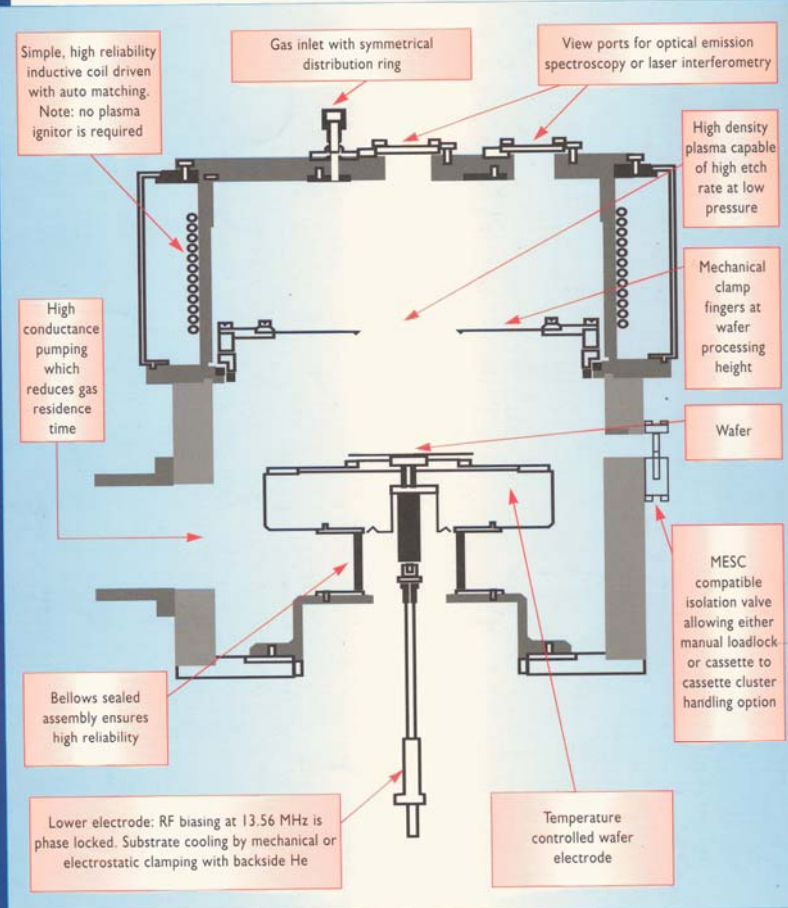
The original STS etcher. (Newer ones by Alcatel, STS, and others have a number of design changes. Etching should be faster. It should be possible to make narrower trenches and holes.)



Multiplex ICP

Conventional plasma sources are unable to meet the progressive demands of modern processes which include higher etch rate and selectivity values, tighter profile control reducing CD and increasing aspect ratio while maintaining minimal microloading and

macroloading effects. An advancement in plasma source design is essential to accomplish realisation of these requirements. The Multiplex Inductively Coupled Plasma (ICP) from Surface Technology Systems provides the solution.



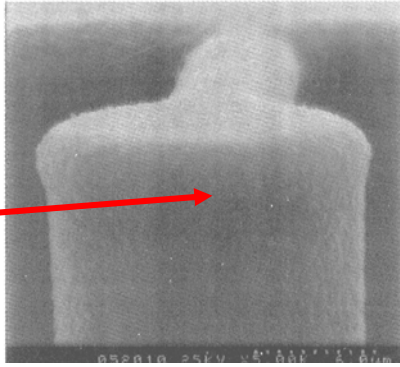
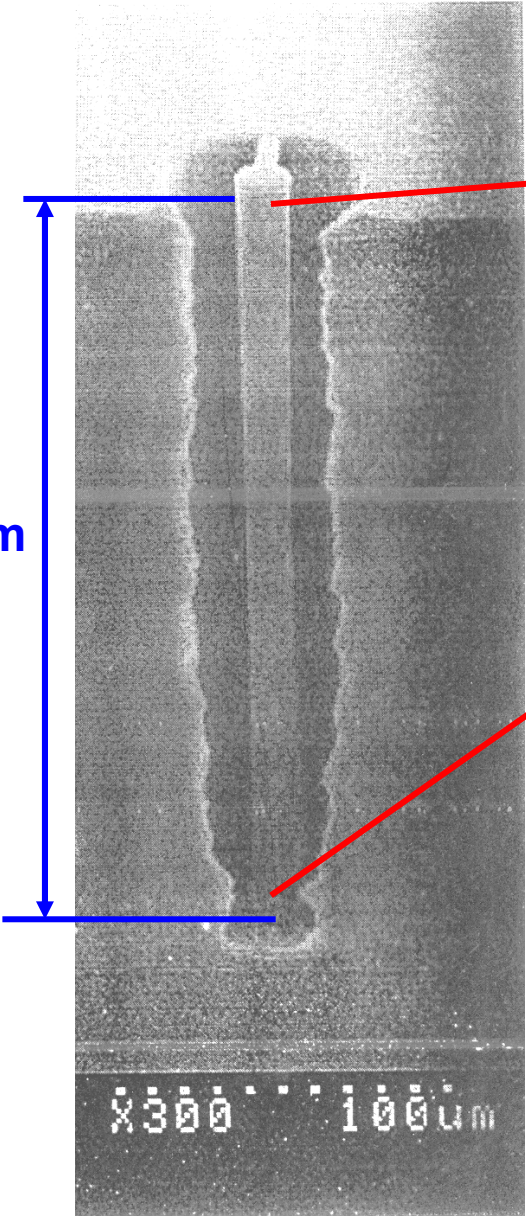
SURFACE TECHNOLOGY SYSTEMS LIMITED PRINCE OF WALES INDUSTRIAL ESTATE ABERCARN NEWPORT, GWENT, NP1 5AR, UK
 TELEPHONE +44 (1493) 249044 FAX: +44 (1493) 249478

(1633) 652400

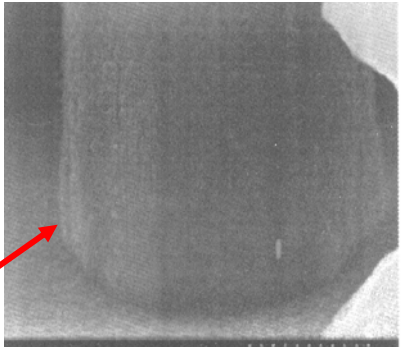
Examples of etching and coating with polysilicon.

An early test structure by Julie Segal, etched and coated (middle, right), showing conformal nature of poly coat.

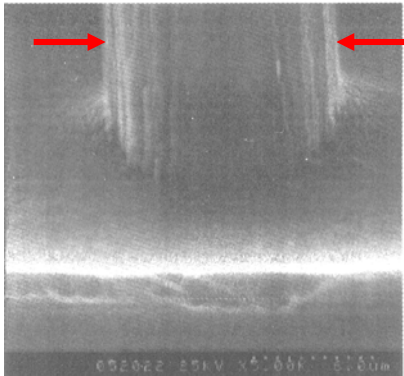
An **electrode hole, filled**, broken (accidentally) in a plane through the axis, showing grain structure (below). The surface poly is later etched off.



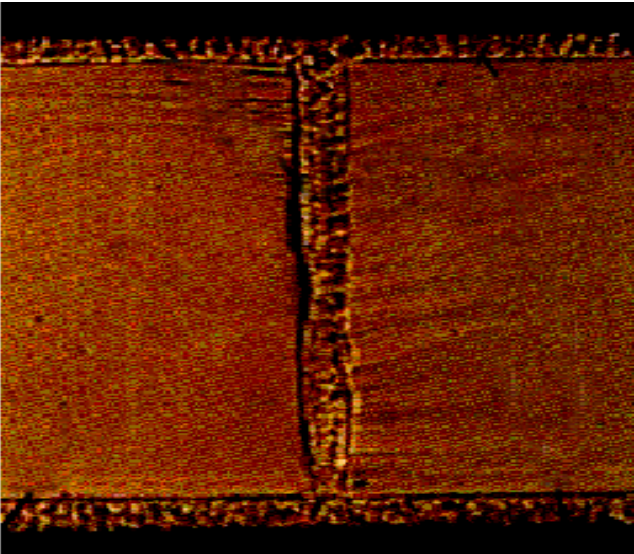
coated, top



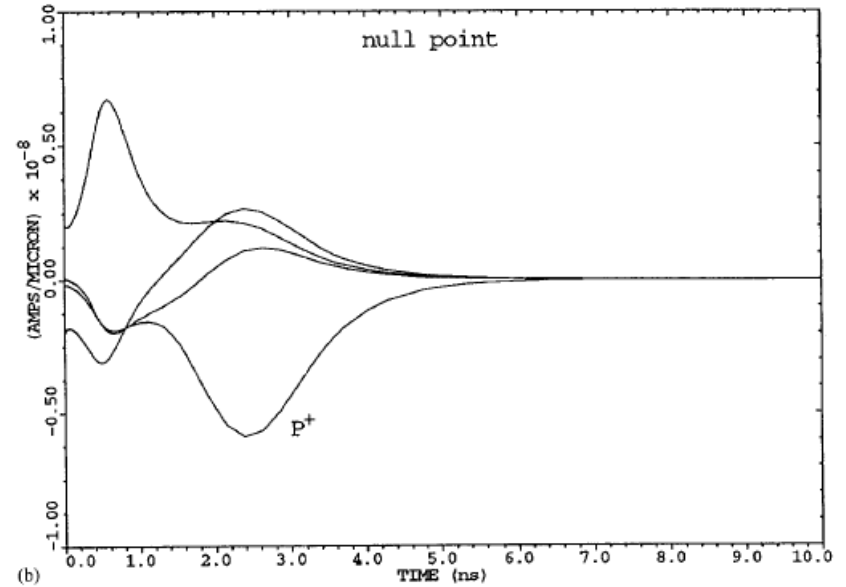
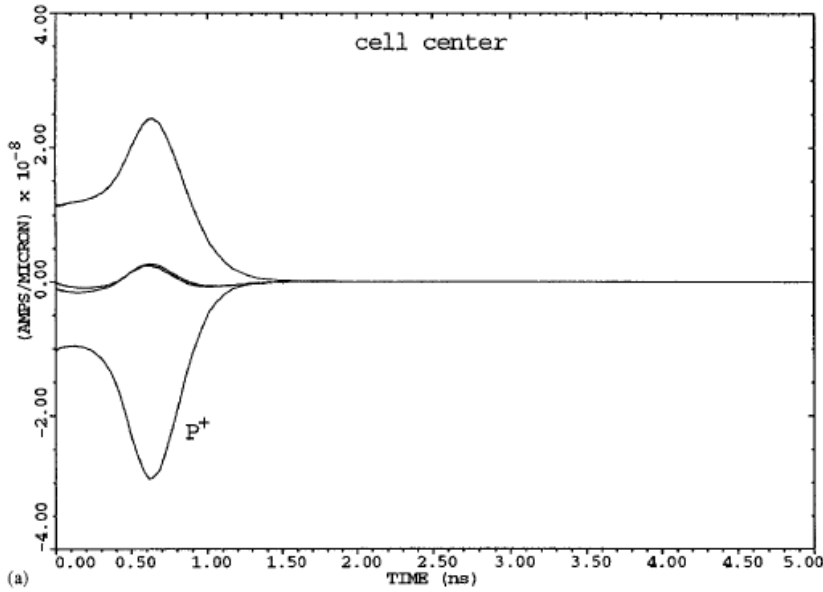
coated, bottom



uncoated

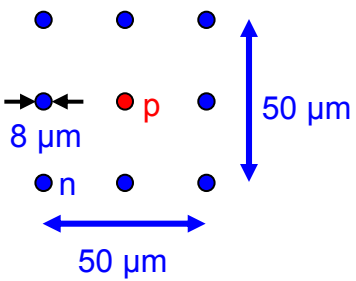


Potential 3D features from preliminary calculations by Julie Segal:



↑
1 ns

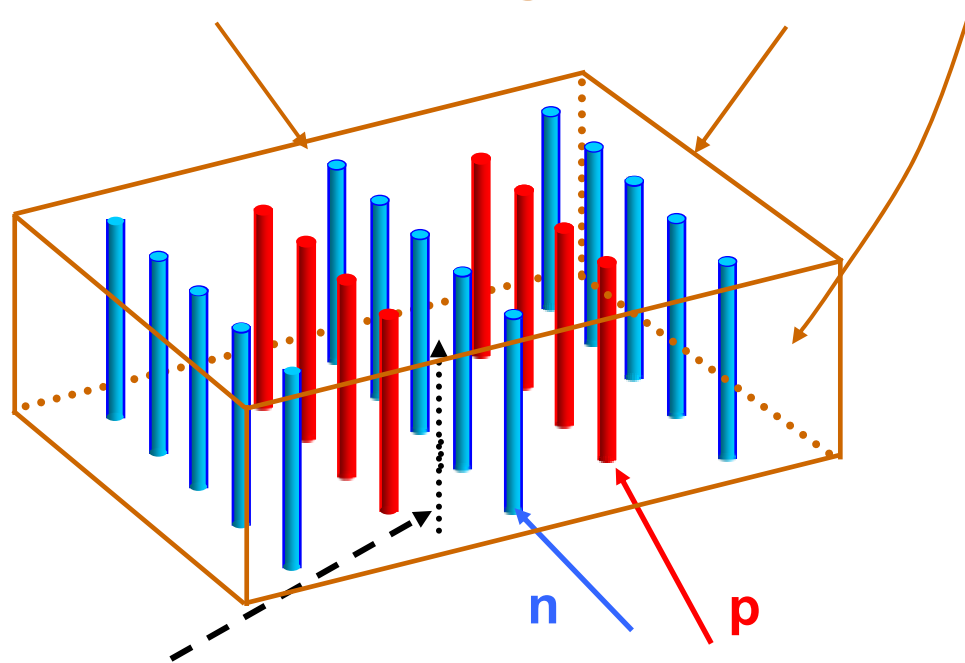
↑
3 ns



3. Fast pulses. Current to the **p** electrode and the other 3 **n** electrodes.

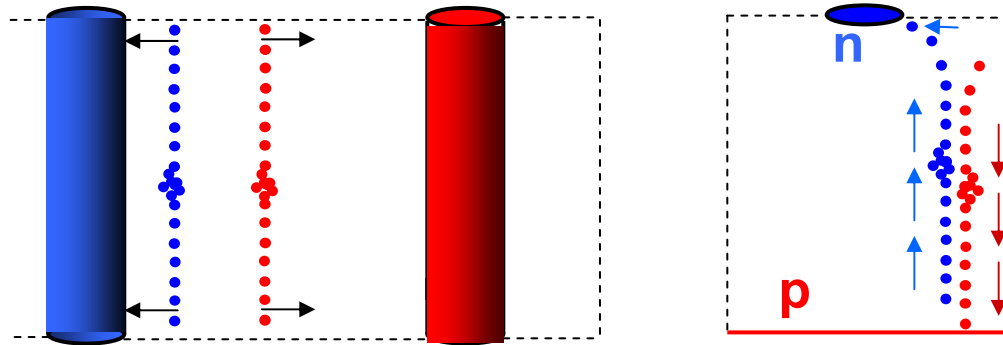
(The track is parallel to the electrodes through a cell center and a null point. $V - \text{bias} = 10\text{V}$. Cell centers are in center of any quadrant. Null points are located between pairs of **n** electrodes.)

p active - edge electrodes



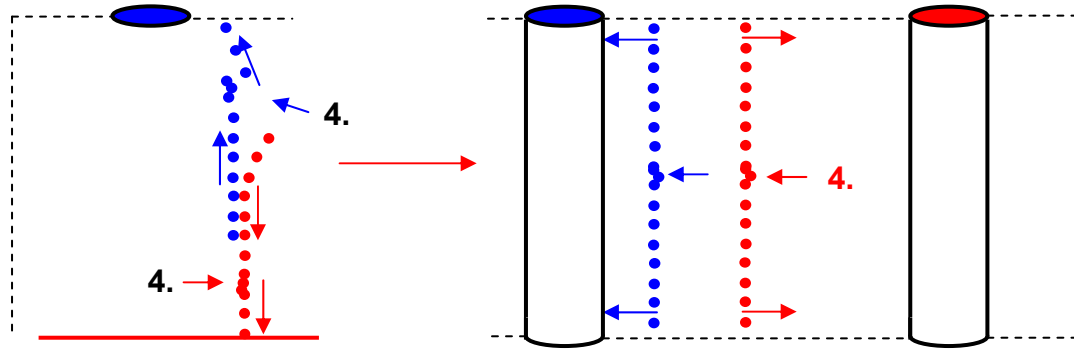
Track

Internal 3D electrodes



3D ← track with δ ray → planar

Speed: planar \longrightarrow 3D



1. 3D lateral cell size can be **smaller** than wafer thickness, so

2. in 3D, field lines end on **electrodes of larger area**, so

3. most of the signal is induced when the charge is close to the electrode, where the electrode solid angle is large, so planar signals are **spread out in time** as the charge arrives, and

4. Landau fluctuations along track arrive **sequentially** and may cause **secondary peaks**

5. if readout has inputs from both n+ and p+ electrodes,

1. **shorter collection distance**

2. **higher average fields for any given maximum field (price: larger electrode capacitance)**

3. **3D signals are concentrated in time as the track arrives**

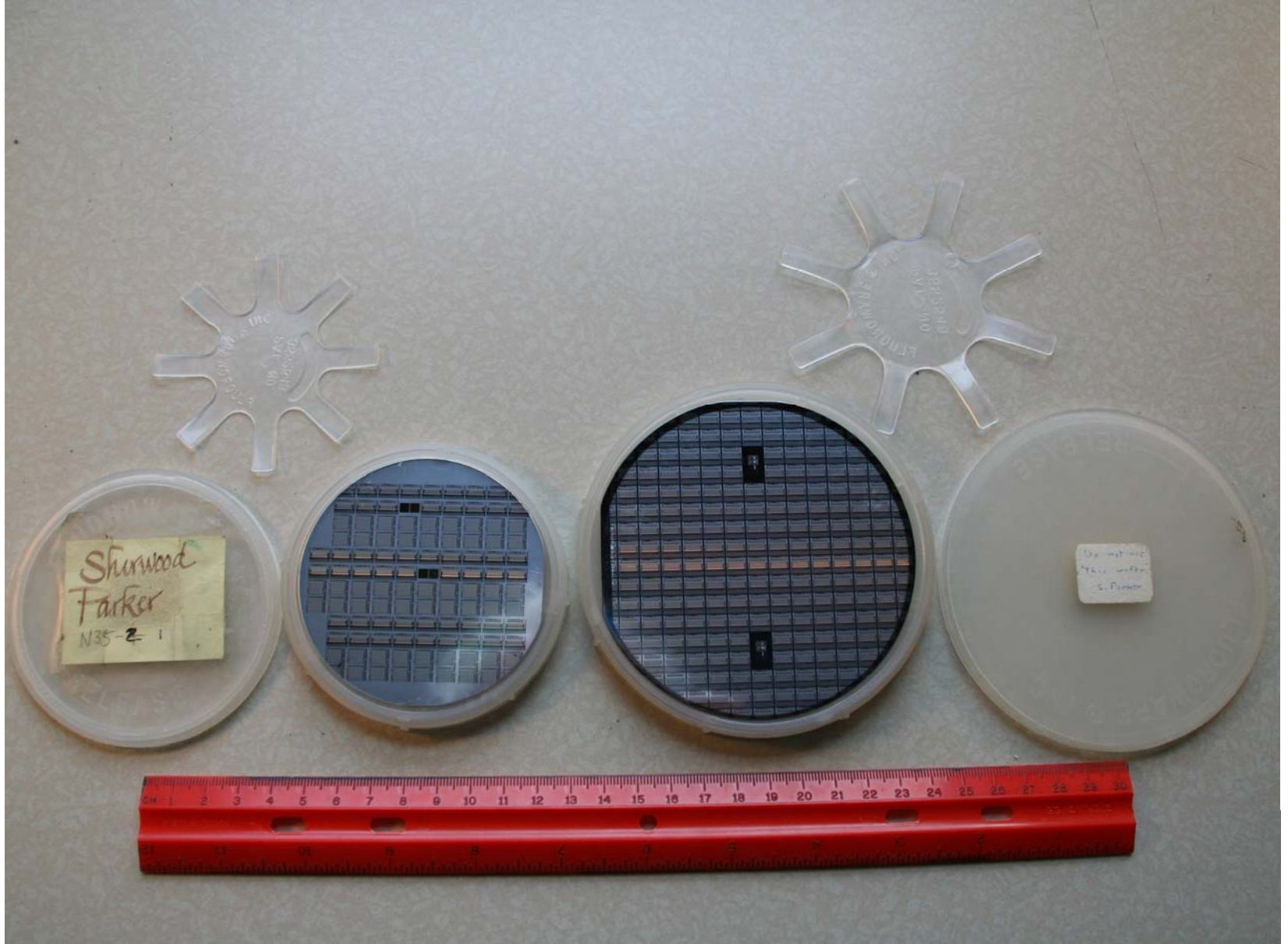
4. **Landau fluctuations (delta ray ionization) arrive nearly simultaneously**

5. **drift time corrections can be made**

1. introduction
2. **history**
3. factors affecting speed
4. generating the signal – Ramo's theorem
5. amplifying the signal – charge and current amplifiers
6. trench electrode sensors
7. hex-cell sensors
8. experimental results
9. analysis – constant fraction discrimination
10. analysis – fitting with almost-noise-free pulses
11. next

A Very Brief History of Ever Shorter Times

- The first silicon radiation sensors were rather slow with large, high capacitance elements. The resultant noise was reduced by integration.
- For example, in the pioneering UA2 experiment at CERN, “the width of the shaped signal is 2 μ s at half amplitude and 4 μ s at the base.” (Faster discrete-component amplifiers were available, but not widely used.)
- The development of microstrip sensors greatly reduced the capacitance between the top and bottom electrodes, adding a smaller, but significant one between adjacent strips.
- The 128-channel, Microplex VLSI readout chip, had amplifiers with 20 – 25 ns rise times, set by the need to roll off amplification well before
 - $\omega t \leq \pi$ (t = time, input to inverted output then fed back to input)
- (Otherwise we would have produced a chip with 128 oscillators and no amplifiers.)
- The planned use of microstrip detector arrays at colliders with short inter-collision times required a further increase in speed.
- Silicon sensors with 3D electrodes penetrating through the silicon bulk allow charge from long tracks to be collected in a rapid, high-current burst.
- Advanced VLSI technology provides ever higher speed current amplifiers. Up to the sensor speed, such signals grow more rapidly with increasing frequency, than white noise.



The first ever custom VLSI silicon microstrip readout chips. Made at Stanford in 1984). (left, 7.5 cm), then by AMI – (right, 10 cm). 11

planar sensor pulse shape

Electrostatic simulations for the design of silicon strip detectors and front-end electronics

R. Sonnenblick, N. Cartiglia, B. Hubbard, J. Leslie, H.F.-W. Sadrozinski and T. Schalk
Santa Cruz Institute for Particle Physics, University of California, Santa Cruz, CA 95064, USA

(an early, successful, attempt to increase speed in the era of 1 μ s shaping times)

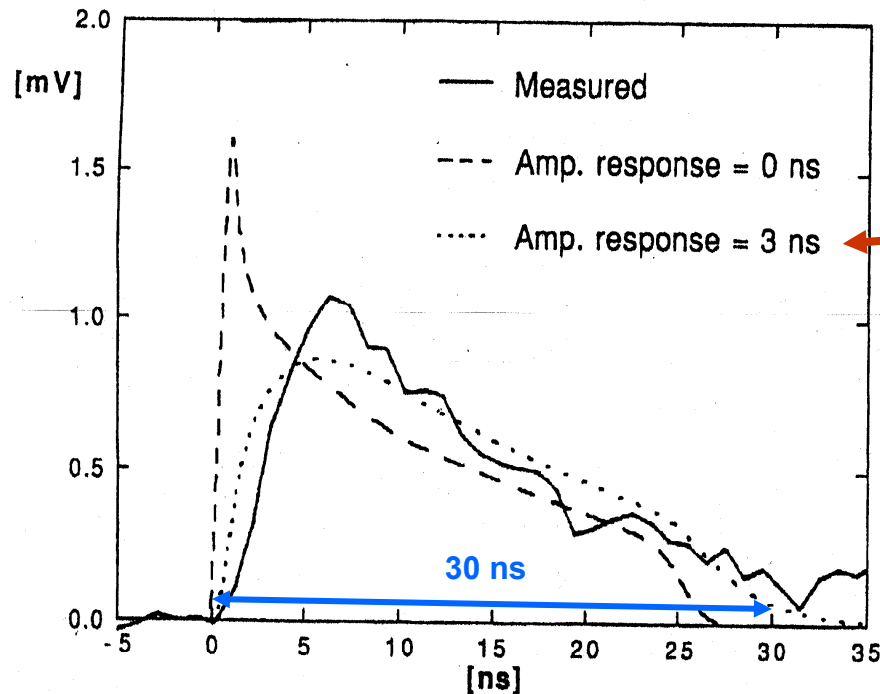


Fig. 3. Pulse shape at the junction side from a minimum ionizing particle. The three curves are the simulated current (with initial diffusion), the simulated current convoluted with the preamplifier response, and a typical observed pulse, respectively.

1. introduction
2. history
3. factors affecting speed
4. generating the signal – Ramo's theorem
5. amplifying the signal – charge and current amplifiers
6. trench electrode sensors
7. hex-cell sensors
8. experimental results
9. analysis – constant fraction discrimination
10. analysis – fitting with almost-noise-free pulses
11. next

Some elements affecting time measurements

- 1. variations in track direction** – 1 and 2 can affect the shape and timing of the detected pulse.
- 2. variations in track location**
- 3. variations in total ionization signal** – can affect the trigger delay.
- 4. variations in ionization location along the track** – **Delta rays** – high energy, but still generally non-relativistic, ionization (“knock-on”) electrons. Give an ever-larger signal when the Ramo weighting function increases as they approach a planar detector electrode, with their current signal dropping to zero as they are collected. This produces a pulse with a leading edge that has changes of slope which vary from event to event, limiting the accuracy of getting a specific time from a specific signal amplitude for the track.
- 5. magnetic field effects affecting charge collection** – $E \times B$ forces shift the collection paths but for 3D-barrel only parallel to the track.
- 6. measurement errors due to noise** – **This currently is the major error source.**
- 7. incomplete use of, or gathering of, available information** – This is a challenge mainly for the data acquisition electronics which, for high speed, will often have to face power and heat removal limitations.
8. In addition, long collection paths for thick planar sensors increase the time needed for readout and decrease the rate capabilities of the system.

- 1. introduction**
- 2. history**
- 3. factors affecting speed**
- 4. generating the signal – Ramo's theorem**
- 5. amplifying the signal – charge and current amplifiers**
- 6. trench electrode sensors**
- 7. hex-cell sensors**
- 8. experimental results**
- 9. analysis – constant fraction discrimination**
- 10. analysis – fitting with almost-noise-free pulses**
- 11. next**

Calculating the signals

1. Calculate E fields using a finite element calculation. (Not covered here.)
2. Calculate track charge deposition using Landau fluctuating value for (dE/dx) divided by 3.62 eV per hole-electron pair.
3. Paths of energetic **delta rays** may be generated using **Casino**, a program from scanning electron microscopy. (GEANT4 may be used for some of 2 and 3.)
4. Calculate velocities and diffusion using C. Jacoboni, et al. "A review of some charge transport properties of silicon" *Solid-State Electronics*, 20 (1977) 7749.
5. Charge motion will induce signals on all electrodes, each of which will affect all the other electrodes. Handle this potential mess with:
6. **Next: charge motion, delta rays, Ramo's theorem.**

DELTA RAYS - 1

$$\frac{d^2n}{dTdx} = 2\pi N_A r_e^2 m_e c^2 \frac{Z}{A} \left(\frac{z}{\beta} \right)^2 \frac{F(T)}{T^2}$$

Integrating over T, the kinetic energy of the delta ray gives the number of delta rays in the 170 μm thickness of the hex sensor with T between T_1 and T_2

(T_{max} is $\approx \text{MeV}$; $1/T_{\text{max}} \approx 0$)

$$T_{\text{max}} = \frac{2m_e c^2 \beta^2 \gamma^2}{1 + 2\gamma m_e / M + (m_e / M)^2} \approx \text{MeV}; 1/T_{\text{max}} \approx 0$$

$$n = 3.03(\text{KeV}) \left(\frac{1}{T_1} - \frac{1}{T_2} \right)$$

**So 3 KeV δ rays are common, 30 KeV uncommon, 300 KeV rare.
Calculate production angles and then look at some of them.**

Angular distribution.

$$\cos \theta = \left(\frac{T}{p} \right) \left(\frac{p_{\max}}{T_{\max}} \right)$$

$$\frac{T}{pc} = \frac{mv^2}{2mvc} = \frac{v}{2c} \approx 0$$

$$\frac{p_{\max}c}{T_{\max}} = \frac{\beta\gamma mc^2}{(\gamma-1)mc^2} = \frac{\beta\gamma}{(\gamma-1)} = \frac{(1-1/\gamma^2)^{1/2} \gamma}{\gamma-1} = \frac{(\gamma^2-1)^{1/2}}{\gamma-1} = \left(\frac{\gamma+1}{\gamma-1} \right)^{1/2} \approx 1$$

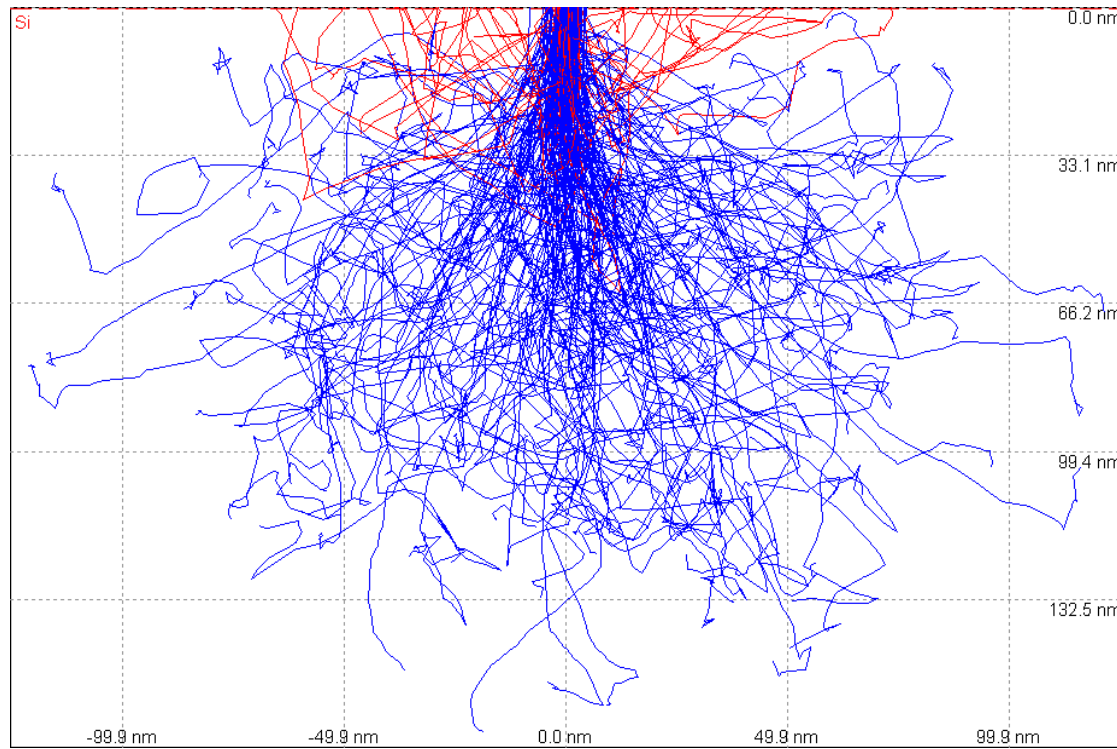
Cos θ is the product of a term near zero – the non-relativistic T/pc – and of a term near one – the relativistic $p_{\max}c/T_{\max}$ – so cos θ is small and the production angle is large.

Starting with the very probable **T = 3 KeV**, and continuing with the increasingly less probable **T = 10, 30, and 60 KeV**, the angles are **86°, 84°, 80°, and 76°**.

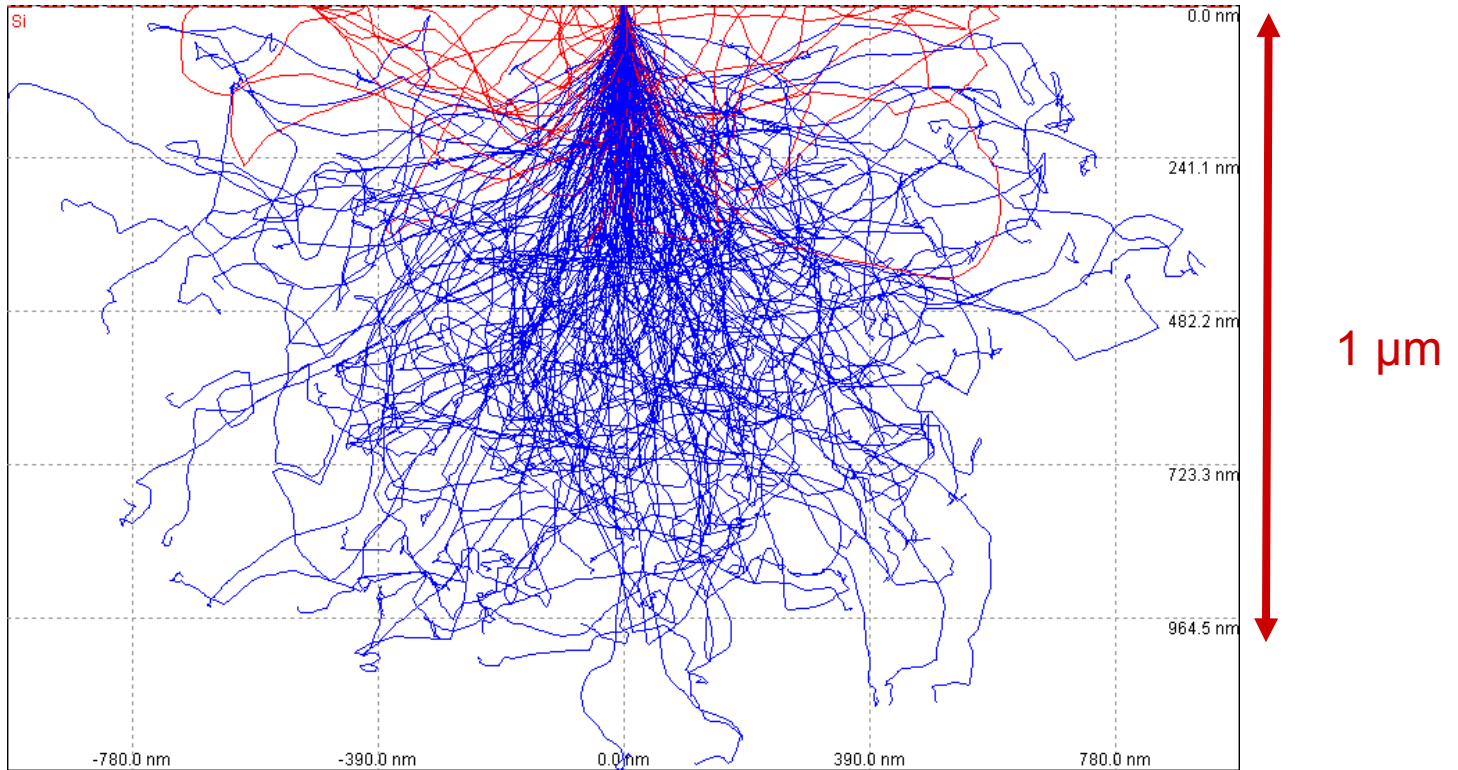
DELTA RAYS - 2

- With electron velocities of about 5×10^6 cm / sec, a delta ray of length $0.5 \mu\text{m}$
- if oriented ahead of the track
- could reach an n electrode up to 10 ps ahead of the main track.
- This will happen above 10 KeV in $\approx 5-10\%$ of events
- These energies will be compared with the mean loss
- $dE/dx_{\text{min, silicon}} = 1664 \text{ KeV} / \text{gm} / \text{cm}^2$ giving
- $\Delta T_{\text{mean}} = 2.329 \times 0.017 \times 1664 = 65.9 \text{ KeV}$.

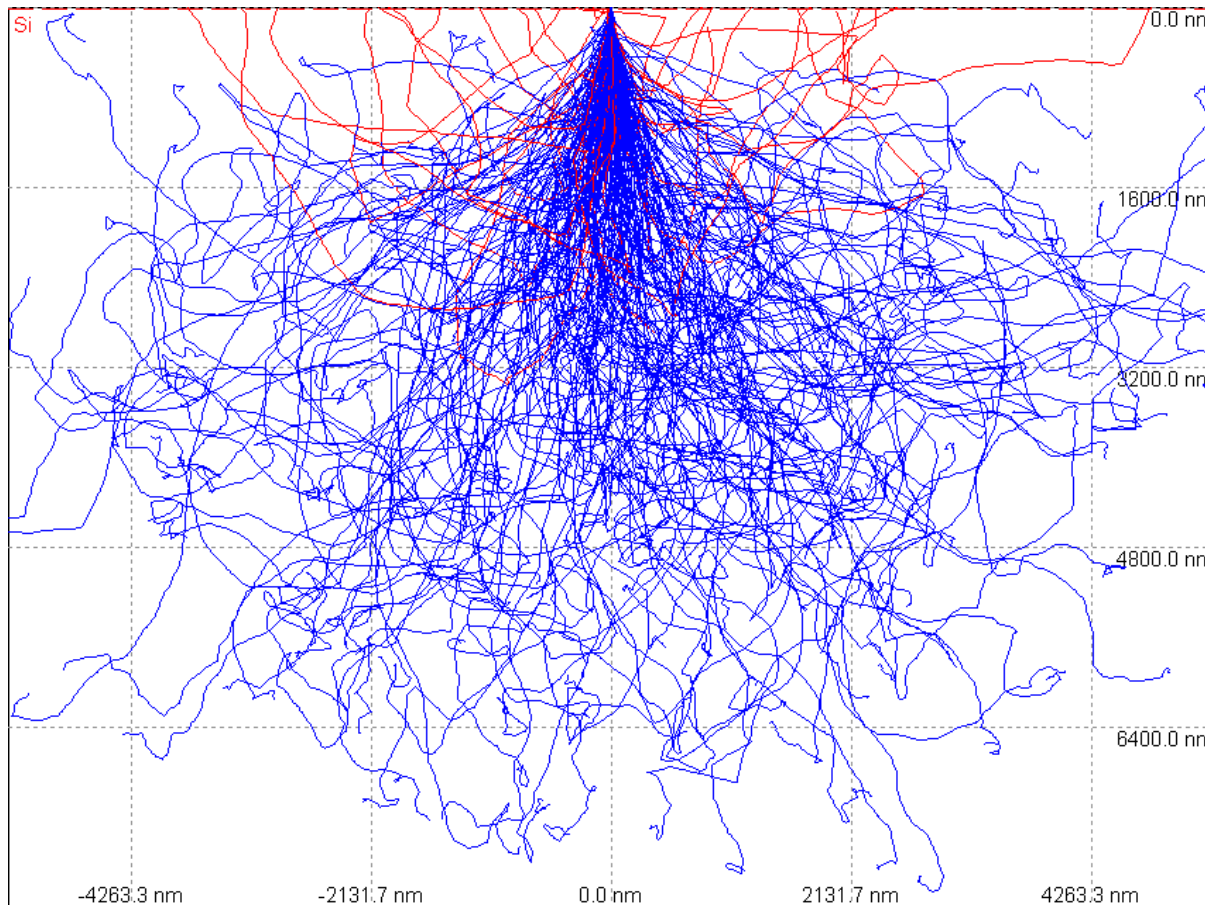
200 3-keV delta rays



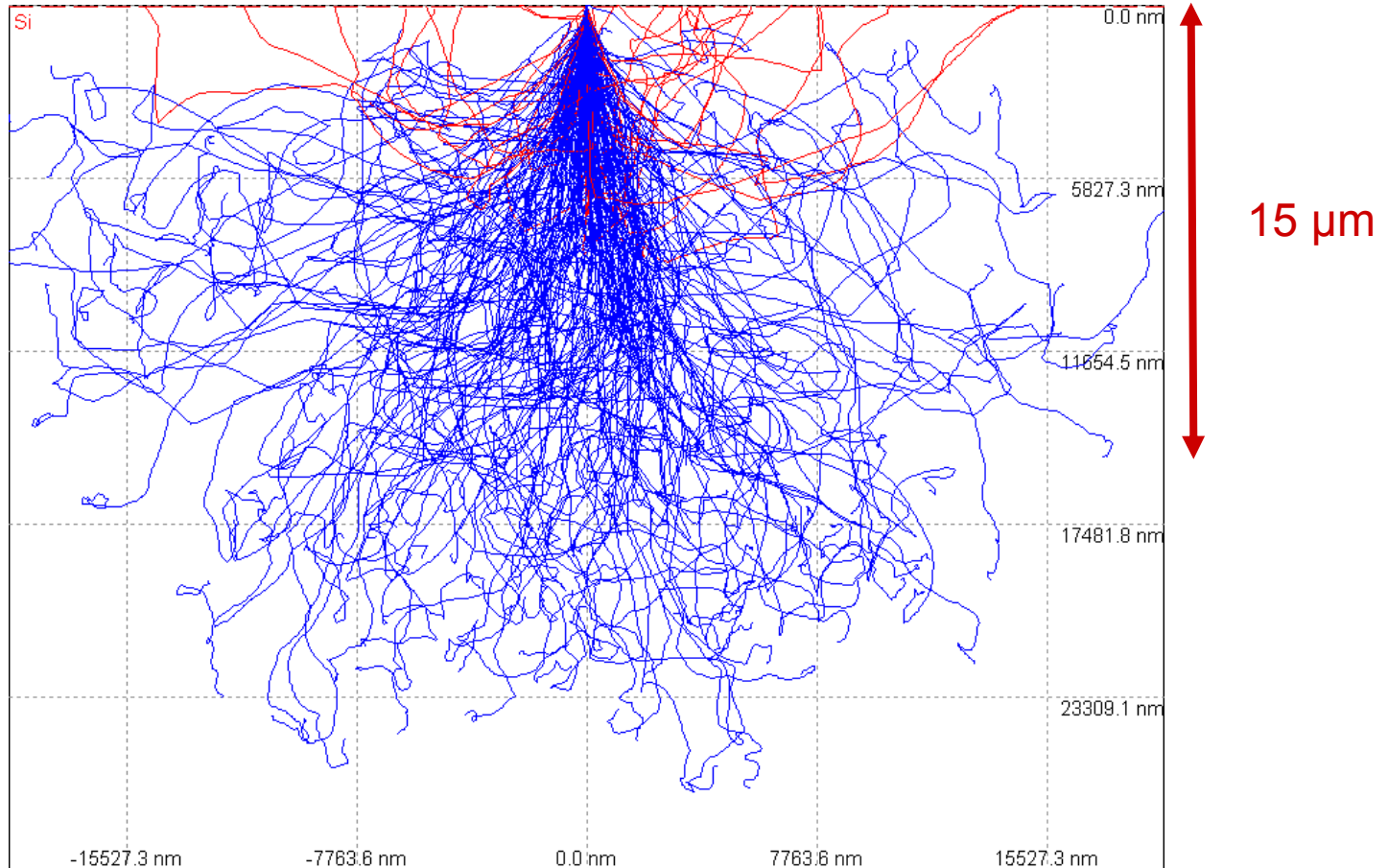
200 10-keV delta rays



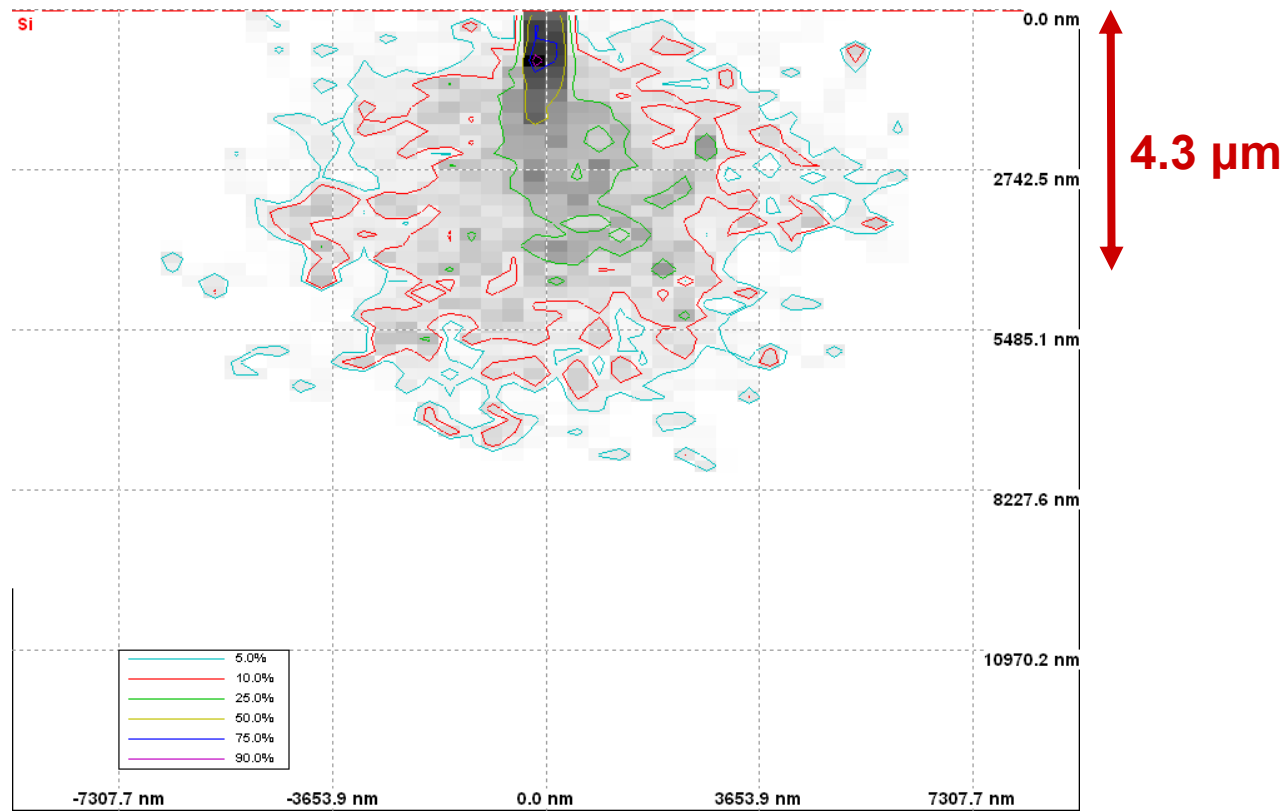
200 30-keV delta rays



200 60-keV delta rays

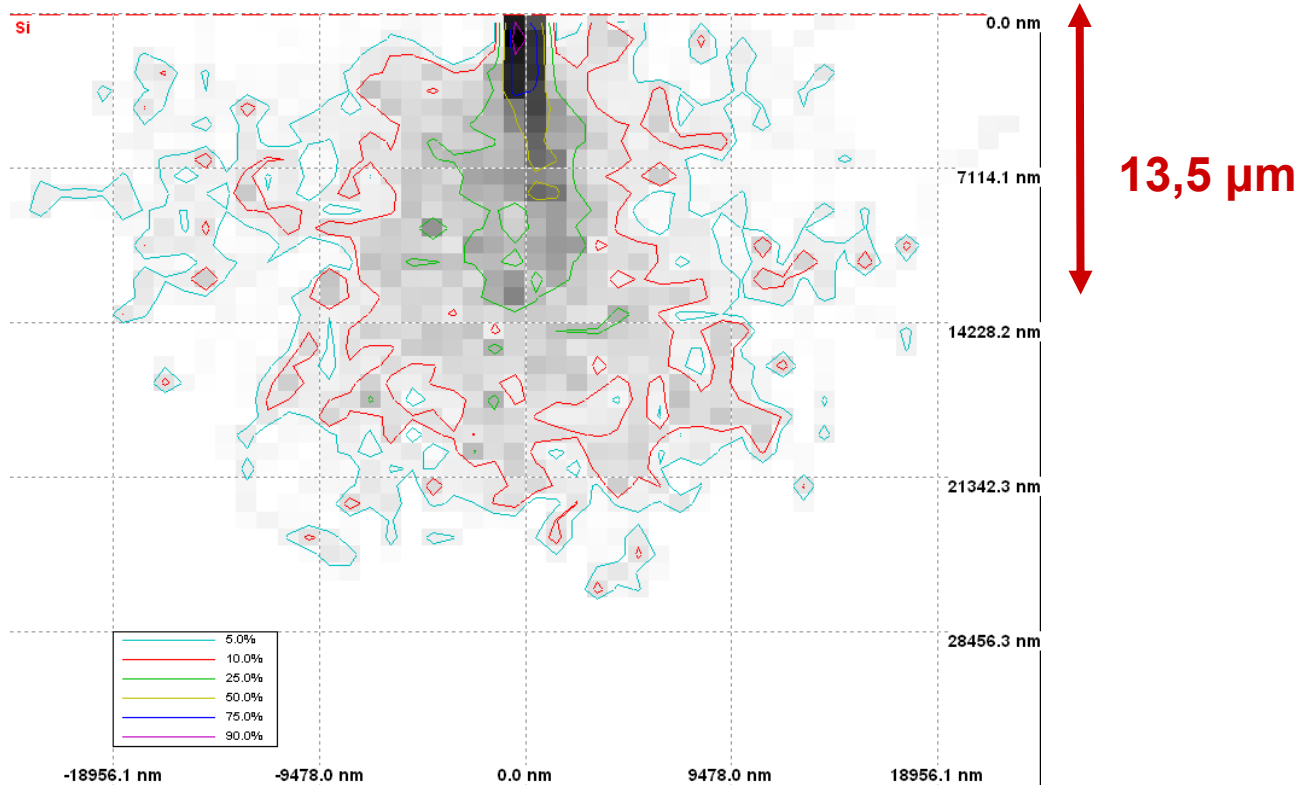


Energy deposition – 30 keV delta rays



50% containment contour depth of 2.0 μm, max full width of 0.8 μm
75% containment contour depth of 4.3 μm, max full width of 2.7 μm

Energy deposition – 60 keV delta rays



50% containment contour depth of 8.0 μm, max full width of 2.0 μm
75% containment contour depth of 13.5 μm, max full width of 7.3 μm

From:

A REVIEW OF SOME CHARGE TRANSPORT PROPERTIES OF SILICON,
 C. JACOBONI, C. CANALI, G. OTIAVIANI and A. ALBERIGI QUARANTA
 (Solid-State Electronics, 1977, Vol. 20, pp. 7749.)

we can get the **drift velocities** for holes and electrons:

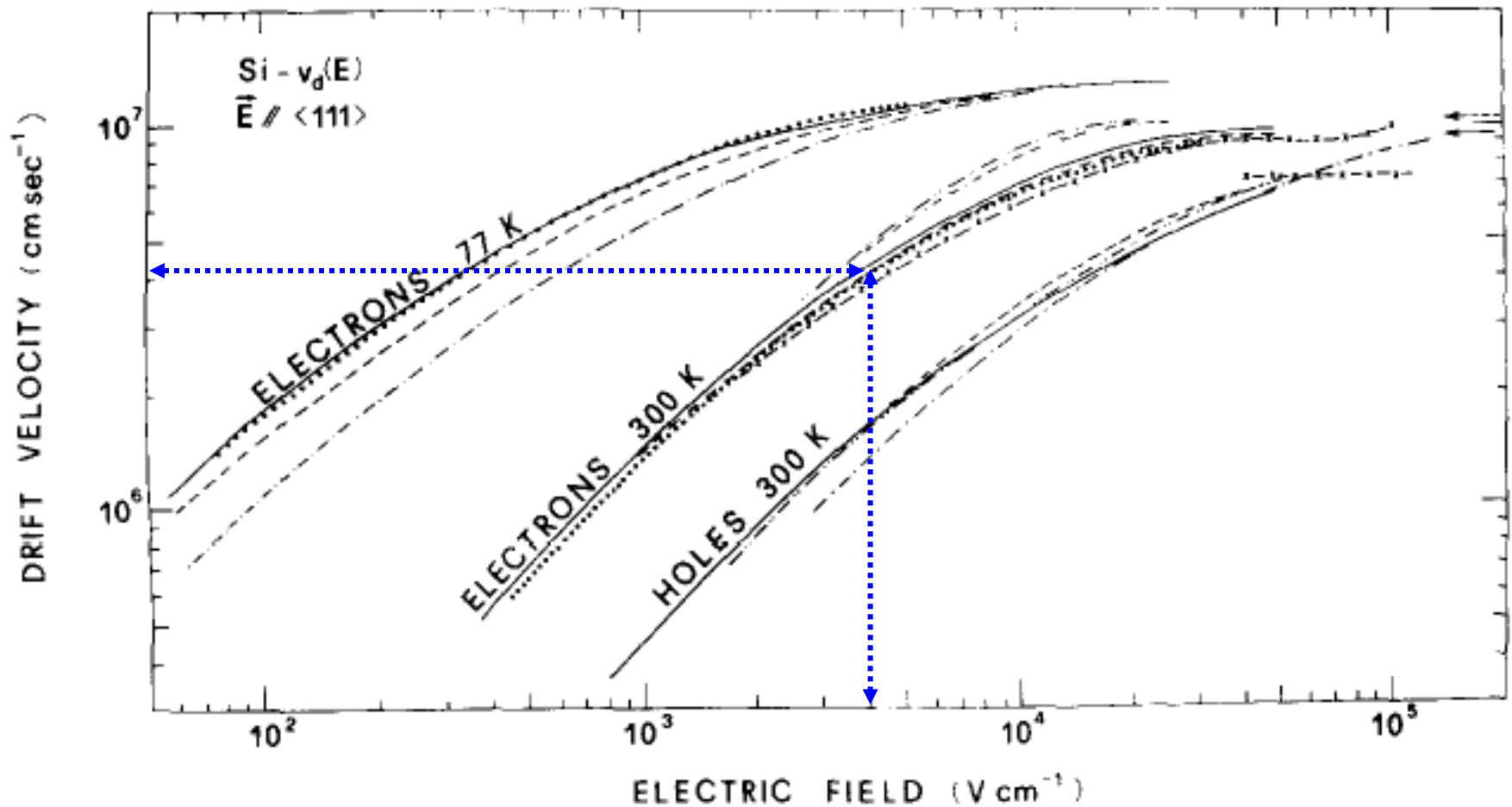
“Figures 15 and 16 show the electron and hole drift velocities as functions of the electric field E applied along a (111) direction at several temperatures, fitted by the equation : ”

$$V_{\text{drift}} = v_m \times (E/E_c) \times [1 + (E/E_c)^\beta]^{-(1/\beta)}$$

with the parameters given in Table 5:

Table 5. Best-fitting parameters for the electric field and temperature dependence of electron and hole drift velocities in high-purity silicon, as given in eqn (9)

	Electrons	Holes	Units
v_m	$1.53 \times 10^9 \times T^{-0.87}$	$1.62 \times 10^8 \times T^{-0.32}$	cm sec ⁻¹
E_c	$1.01 \times T^{1.33}$	$1.24 \times T^{1.68}$	V cm ⁻¹
β	$2.57 \times 10^{-2} \times T^{0.66}$	$0.46 \times T^{0.17}$	—
<i>T</i> is measured in degrees Kelvin			



A REVIEW OF SOME CHARGE TRANSPORT PROPERTIES OF SILICON†

Solid-State Electronics, 1977, Vol. 20, pp. 77-89.

C. JACOBONI, C. CANALI, G. UTTAVIANI and A. ALBERIGI QUARANTA
 Istituto di Fisica dell'Università di Modena, 41100 Modena, Italy

The formula is for $\langle 111 \rangle$ silicon, but the graphs below show that at non-cryogenic temperatures, there is not much variation in drift velocities with direction (dashed line $\langle 111 \rangle$, solid line $\langle 100 \rangle$)

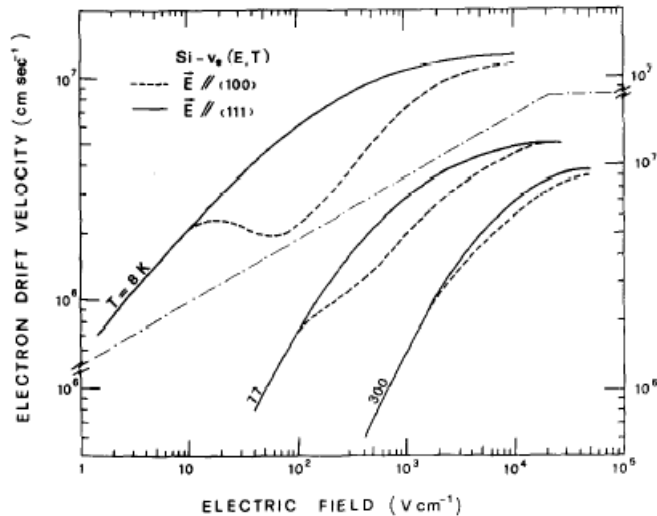


Fig. 7. Experimental results[8, 28] of electron drift velocity as a function of the electric field applied parallel to $\langle 11 \rangle$ and $\langle 100 \rangle$ crystallographic directions at several temperatures.

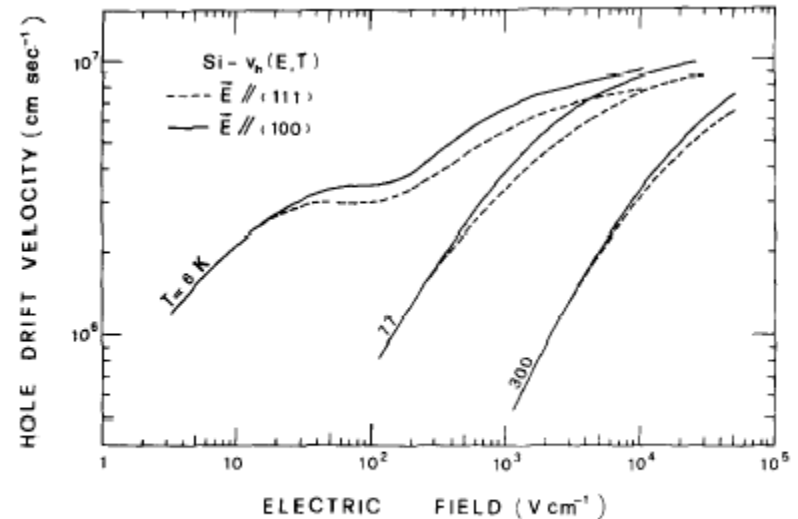
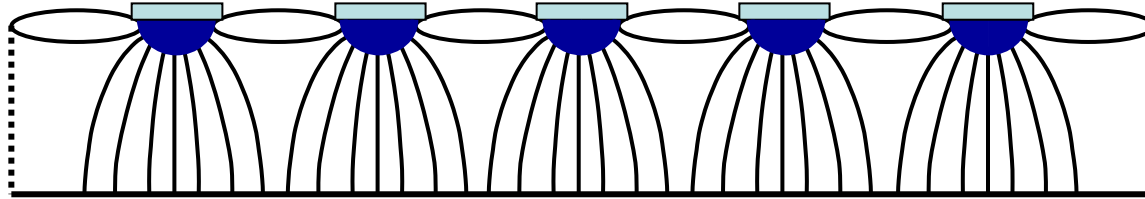


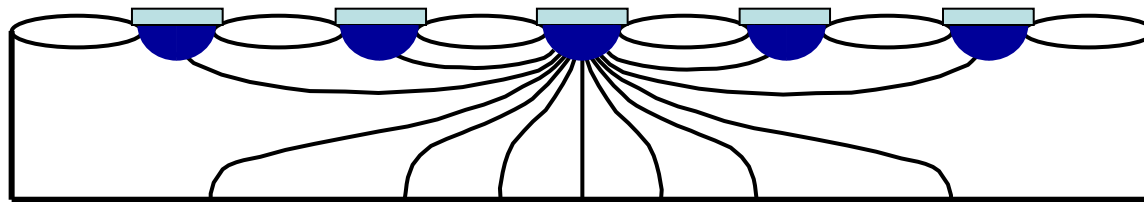
Fig. 8. Experimental results[11, 28] of hole drift velocities as functions of the electric field applied parallel to $\langle 111 \rangle$ and $\langle 100 \rangle$ crystallographic directions at several temperatures.

Ramo's theorem: to calculate the current induced on any electrode

1. Calculate the true fields and from them the charge velocity, v .



2. Calculate the weighting field, E_w , resulting from placing 1 V on the signal electrode and 0 V on all other electrodes. (The weighting field is usually largest near the signal electrode. The large solid angle there intercepts more of the moving-charge's field lines.)



3. The induced current, I , will be the dot product of the velocity vector with the (dimensionless) weighting field: $I = q v \cdot E_w$

And here are some references:

1. Simon Ramo, “Currents Induced by Electron Motion”, *Proceedings of the I.R.E.*, **27** (1939) 584. **Next slide.**
2. W. Shockley, “Currents to Conductors Induced by a Moving Point Charge”, *Journal of Applied Physics*, **9** (1938) 635. **Done independently, but not nearly as nicely as Ramo’s paper.**
3. G. Cavalleri, E. Gatti, G. Fabri, and V. Svelto, ” Extension Of Ramo's Theorem As Applied To Induced Charge In Semiconductor Detectors”, *Nuclear Instruments and Methods* **92** (1971) 137. **Leaving the era of vacuum tubes, adds material.**
4. E. Gatti, A. Geraci, “Considerations about Ramo’s theorem extension to conductor media with variable dielectric constant”, Letter to the Editor, *Nuclear Instruments and Methods in Physics Research A* **525** (2004) 623–625.

Currents Induced by Electron Motion*

SIMON RAMO†, ASSOCIATE MEMBER, I.R.E.

Summary—A method is given for computing the instantaneous current induced in neighboring conductors by a given specified motion of electrons. The method is based on the repeated use of a simple equation giving the current due to a single electron's movement and is believed to be simpler than methods previously described.

INTRODUCTION

IN designing vacuum tubes in which electron transit-time is relatively long, it becomes necessary to discard the low-frequency concept that the instantaneous current taken by any electrode is proportional to the number of electrons received by

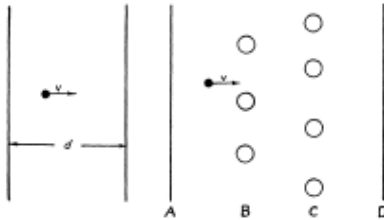


Fig. 1 Fig. 2

it per second. Negative grids, it is known, may carry current even though they collect no electrons and current may be noted in the circuit of a collector during the time the electron is still approaching the collector. A proper concept of current to an electrode must consider the instantaneous change of electrostatic flux lines which end on the electrode and the methods given in the literature for computing induced current due to electron flow are based on this concept.

A method of computing the induced current for a specified electron motion is here explained which is believed to be more direct and simpler than methods previously described. In the more difficult cases, in which flux plots or other tedious field-determination methods must be used, only one field plot is needed by the present method while the usual methods require a large number.

* Decimal classification: R138. Original manuscript received by the Institute, September 16, 1938.

† General Engineering Laboratory, General Electric Company, Schenectady, N. Y.

METHOD OF COMPUTATION

The method is based on the following equation, whose derivation is given later:

$$i = E_e \epsilon v \tag{1}$$

where i is the instantaneous current received by the given electrode due to a single electron's motion, ϵ is the charge on the electron, v is its instantaneous velocity, and E_e is the component in the direction v of that electric field which would exist at the electron's instantaneous position under the following circumstances: electron removed, given electrode raised to unit potential, all other conductors grounded. The equation involves the usual assumptions that induced currents due to magnetic effects are negligible and that the electrostatic field propagates instantaneously.

SIMPLE EXAMPLE

A simple example is offered in the computation of the instantaneous current due to an electron's motion between two infinite plates (Fig. 1). (The result is a starting point for the analysis of a diode, for example, when the transit-time is long.)

From (1) we obtain immediately

$$i = \epsilon v E_e = \frac{\epsilon v}{d}$$

In the literature¹ it is stated that this same result is deduced from image theory. This involves the setting up of an infinite series of image charges on each side of the plates for a given position of the electron and a consideration of the total flux crossing one of the planes due to the series of charges, a method which is lengthy and requires no little familiarity with methods of handling infinite series.

THE GENERAL CASE

Consider a number of electrodes, A, B, C, D , in the presence of a moving electron (Fig. 2) whose path and instantaneous velocity are known. A tedious way to find the current induced in, say, electrode

¹ D. O. North, "Analysis of the effects of space charge on grid impedance," PROC. I.R.E., vol. 24, pp. 108-158; February, (1936).

A is to make a flux plot of the lines of force emanating from the electron, when it is at some point of its path, and note the portion of the total lines which end on A . By making a number of such plots it is possible to observe the change in the number of lines ending on A as the electron moves, and consequently to compute the induced current. The accuracy is dependent upon the number of plots made.

It is much simpler to use (1). One plot is made for the case of A at unit potential, B, C, D grounded, and the electron removed, E_e is then known and

$$i = E_e \epsilon v.$$

To minimize the induced current in a negative grid, an important consideration in the design of high-frequency amplifiers and oscillators, it may be that (1) will prove helpful to the designer. The equation states that the electrode configuration should be such as to yield minimum E_e . If the electron's path, for example, is made to coincide with an equipotential of the grid (not an equipotential in the field in which the electron is traveling, of course, but an equipotential in that artificial field due to unit potential on the grid, the electron removed, and all else grounded) the induced current will be zero. It will not be possible to realize this for the complete electronic path, since the electron must start at some equipotential surface, but it may be possible to find practical configurations that will approach this condition over a good share of the path.

DERIVATION OF EQUATION (1)

Consider the electron, of charge ϵ , in the presence of any number of grounded conductors, for one of which, say A , the induced current is desired. Surround the electron with a tiny equipotential sphere. Then if V is the potential of the electrostatic field, in the region between conductors

$$\nabla^2 V = 0$$

where ∇^2 is the Laplacian operator. Call V_s the potential of the tiny sphere and note that $V=0$ on the conductors and

$$-\int_{\text{sphere's surface}} \frac{\partial V}{\partial n} ds = 4\pi\epsilon \tag{Gauss' law}$$

where $\partial V/\partial n$ indicates differentiation with respect to the outward normal to the surface and the integral is taken over the surface of the sphere.

Now consider the same set of conductors with the electron removed, conductor A raised to unit potential, and the other conductors grounded. Call the potential of the field in this case V' , so that $\nabla^2 V' = 0$ in the space between conductors, including the point

where the electron was situated before. Call the new potential of this point V'_s .

Now Green's theorem² states that

$$\int_{\text{volume between boundaries}} [V' \nabla^2 V - V \nabla^2 V'] dy = - \int_{\text{boundary surfaces}} \left[V' \frac{\partial V}{\partial n} - V \frac{\partial V'}{\partial n} \right] ds. \tag{2}$$

Choose the volume to be that bounded by the conductors and the tiny sphere. Then the left-hand side is zero and the right-hand side may be divided into three integrals:

- (1) Over the surfaces of all conductors except A . This integral is zero since $V = V' = 0$ on these surfaces.
- (2) Over the surface of A . This reduces to $-\int_{\text{surface } A} (\partial V/\partial n) ds$, for $V' = 1$ and $V = 0$ for conductor A . It will not be possible to realize this for the complete electronic path, since the electron must start at some equipotential surface, but it may be possible to find practical configurations that will approach this condition over a good share of the path.
- (3) Over the surface of the sphere. This becomes $-V'_s \int_{\text{sphere's surface}} \frac{\partial V}{\partial n} ds + V_s \int_{\text{sphere's surface}} \frac{\partial V'}{\partial n} ds$.

The second of these integrals is zero by Gauss' law since $\int (\partial V'/\partial n) ds$ is the negative of the charge enclosed (which was zero for the second case in which the electron was removed).

Finally, we obtain from (2)

$$0 = - \int_{\text{surface } A} \frac{\partial V}{\partial n} ds - V'_s \int_{\text{sphere's surface}} \frac{\partial V}{\partial n} ds = 4\pi Q_A + 4\pi\epsilon V'_s$$

or

$$Q_A = -\epsilon V'_s$$

$$i_A = \frac{dQ_A}{dt} = -\epsilon \frac{dV'_s}{dt} = -\epsilon \left[\frac{\partial V'_s}{\partial x} \frac{dx}{dt} \right]$$

where x is the direction of motion.

Now

$$\frac{dx}{dt} = v \quad \text{and} \quad \frac{\partial V'_s}{\partial x} = -E_x,$$

so

$$i = \epsilon v E_x. \tag{1}$$

² J. H. Jeans, "Electricity and Magnetism," page 160, Cambridge, London, England, (1927).

This is the entire paper.

You may show it to any graduate student (like me, once) who thinks Green's theorem is useless.

Ramo's (and Shockley's) theorem.

Velocities, diffusion, and collection times for a 100 μm parallel-plate trench electrode gap.

	electrons		holes		units
temperature	293.15	245*	293.15	245	$^{\circ}\text{K}$
V ($E = 0.5 \text{ V} / \mu\text{m}$)	4.93	7.0	2.07	2.22	$\text{cm}/\mu\text{s}$
t ($E = 0.5 \text{ V} / \mu\text{m}$)	2.03	1.61	4.84	3.53	ns
σ_t , (parallel diffusion)	0.059		0.16		ns
V ($E = 1.0 \text{ V} / \mu\text{m}$)	6.91	8.8	3.46	4.62	$\text{cm}/\mu\text{s}$
t ($E = 1.0 \text{ V} / \mu\text{m}$)	1.45	1.21	2.89	2.22	ns
σ_t , (parallel diffusion)	0.029		0.06		ns
3 KeV δ ray ($1 \text{ V} / \mu\text{m}$)	1.9	1.5	3.8	2.8	ps
10 KeV δ ray ($1 \text{ V} / \mu\text{m}$)	14	11	29	22	ps
30 KeV δ ray ($1 \text{ V} / \mu\text{m}$)	101	80	202	152	ps
60 KeV δ ray ($1 \text{ V} / \mu\text{m}$)	362	284	723	541	ps

Calculations based on material in:

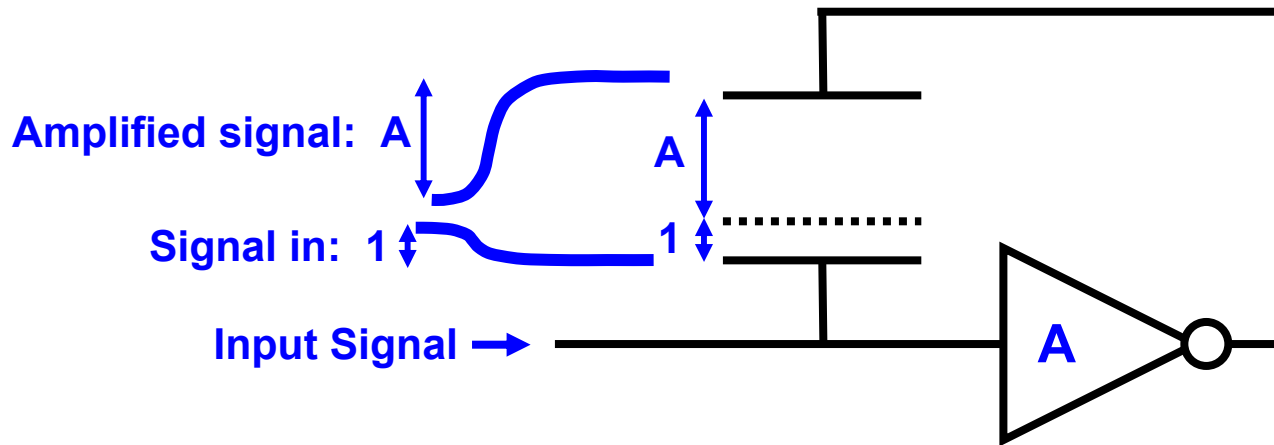
A REVIEW OF SOME CHARGE TRANSPORT PROPERTIES OF SILICON

Solid-State Electronics 20 (1977) 77 – 89

- 1. introduction**
- 2. history**
- 3. factors affecting speed**
- 4. generating the signal – Ramo's theorem**
- 5. amplifying the signal – charge and current amplifiers**
- 6. trench electrode sensors**
- 7. hex-cell sensors**
- 8. experimental results**
- 9. analysis – constant fraction discrimination**
- 10. analysis – fitting with almost-noise-free pulses**
- 11. next**

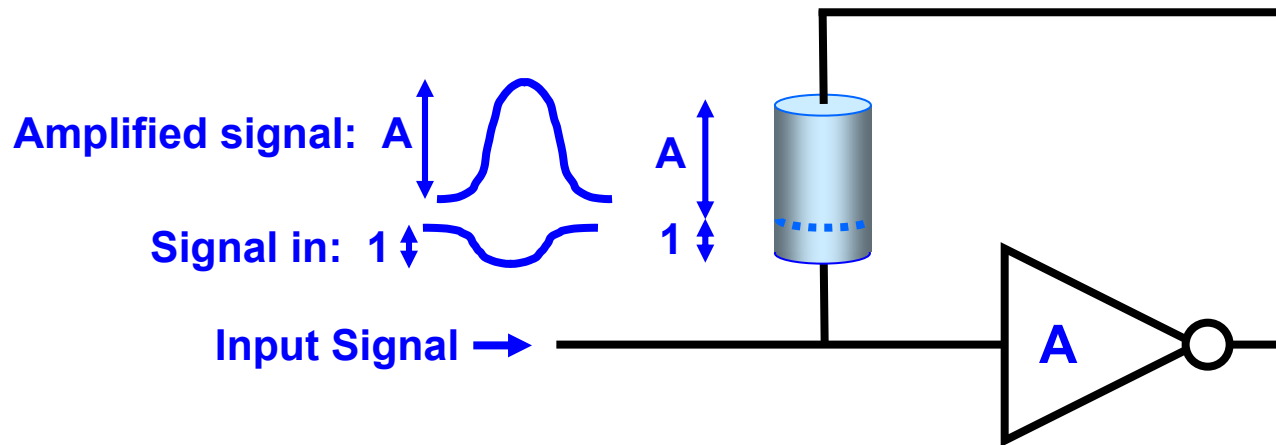
Getting the charge off the large electrodes and onto much smaller transistors:

(In a passive circuit, the charge will divide in proportion to the capacitance, spreading to nearby electrodes.)



After the fed-back signal reaches the integrating capacitor, there will be an effective ground plane $1/(A+1)$ of the way up, making an effective input capacitance $(A+1)$ times thinner and so $(A+1)$ times larger.

In effect, the large output voltage reaching the feedback capacitor pulls the charge in, (Not covered here: removing reset noise.)



1. The same is true of current amplifiers which use resistive feedback elements (including the channel resistance of a fast transistor) generating a voltage proportional to the sensor current.
2. The input resistance is reduced by a factor of $(A+1)$ which is useful for speed as well as pulling off all the charge from the sensor element.
3. Amplifier speed, up to the sensor speed, also increases the signal size.
4. However, to prevent noise-induced oscillation, the amplification must roll off approaching frequencies whose half-period time is less than the feedback time.

**0.13 μm chips now fabricated and used here
rise, fall times \approx 1.5 ns**

A high-speed low-noise transimpedance amplifier in a 0.25 μm CMOS technology

Giovanni Anelli^{a,*}, Kurt Borer^b, Luca Casagrande^a, Matthieu Despeisse^a, Pierre Jarron^a,
Nicolas Pelloux^a, Shahyar Saramad^{a,c} **rise times \approx 3.5 ns** **fall times \approx 3.5 ns**

^a CERN, EP Division, CH-1211 Geneva 23, Switzerland

^b University of Bern, Laboratory for High Energy Physics, Sidlerstr. 5, CH-3012 Bern, Switzerland

^c Institute for Studies in Theoretical Physics and Mathematics (IPM), Tehran, Iran, P.O. Box 19395-5531

Elsevier use only: Received date here; revised date here; accepted date here

Abstract

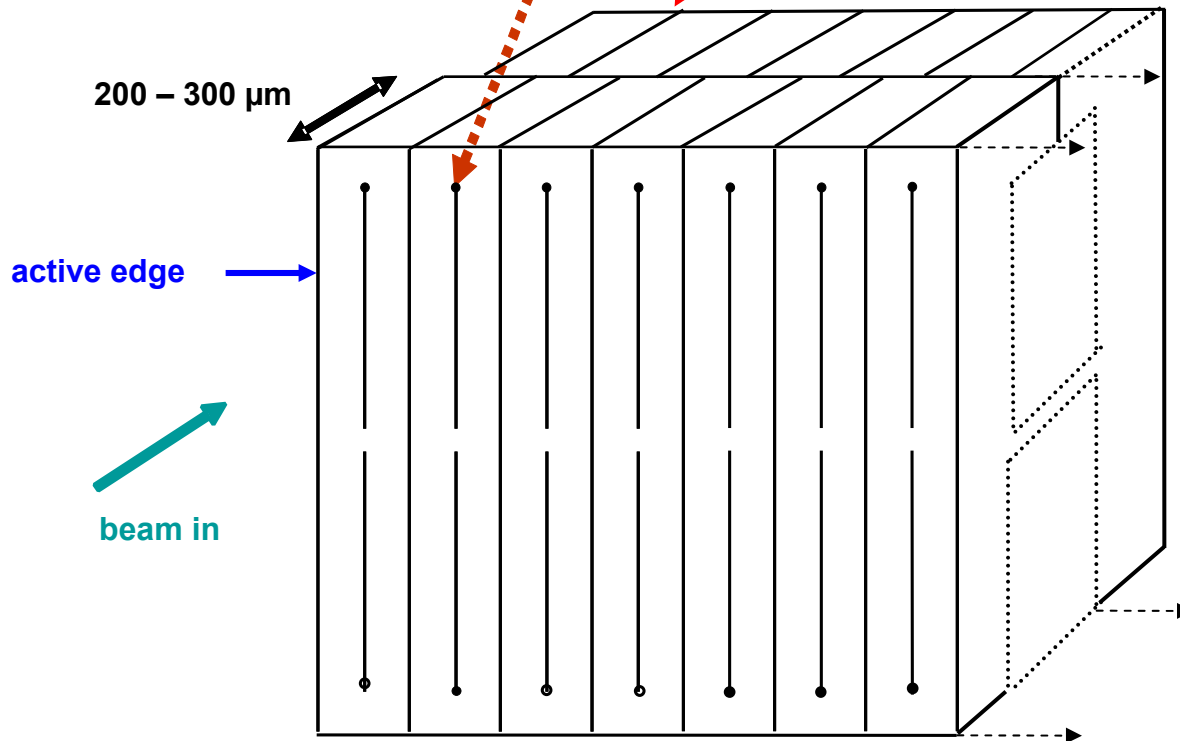
We present the simulated and measured performance of a transimpedance amplifier designed in a quarter micron CMOS process. Containing only NMOS and PMOS devices, this amplifier can be integrated in any submicron CMOS process. The main feature of this design is that a transistor in the feedback path substitutes the transresistance. The circuit has been optimized for reading signals coming from silicon strip detectors with few pF input capacitance. For an input charge of 4 fC, an input capacitance of 4 pF and a transresistance of 135 k Ω , we have measured an output pulse fall time of 3 ns and an Equivalent Noise Charge (ENC) of around 350 electrons rms. In view of a utilization of the chip at cryogenic temperatures, measurements at 130 K have also been carried out, showing an overall improvement in the performance of the chip. Fall times down to 1.5 ns have been measured. An integrated circuit containing 32 channels has been designed and wire-bonded to a silicon strip detector and successfully used for the construction of a high-intensity proton beam hodoscope for the NA60 experiment. The chip has been laid out using special techniques to improve its radiation tolerance, and it has been irradiated up to 10 Mrd (SiO₂) without showing any degradation in the performance. © 2002 Elsevier Science. All rights reserved

Keywords: Deep submicron; CMOS; Transimpedance amplifier; Radiation tolerance; Low temperature CMOS

- 1. introduction**
- 2. history**
- 3. factors affecting speed**
- 4. generating the signal – Ramo's theorem**
- 5. amplifying the signal – charge and current amplifiers**
- 6. trench electrode sensors**
- 7. hex-cell sensors**
- 8. experimental results**
- 9. analysis – constant fraction discrimination**
- 10. analysis – fitting with almost-noise-free pulses**
- 11. next**

signal electrodes with contact pads to readout

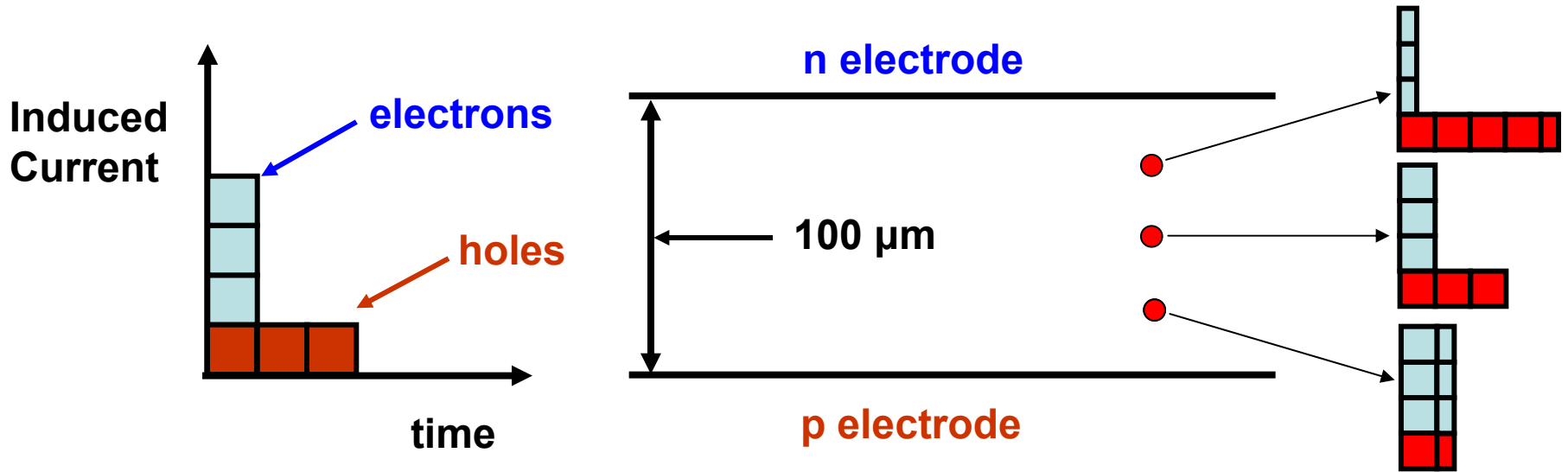
next section offset so signal electrodes do not line up



Schematic diagram of part of one section of two of the planes in an active-edge 3D trench-electrode detector. Other offsets ($\frac{1}{3}$, $\frac{2}{3}$, 0, $\frac{1}{3}$, $\frac{2}{3}$..etc.) may also be used.

A trench-electrode sensor will have:

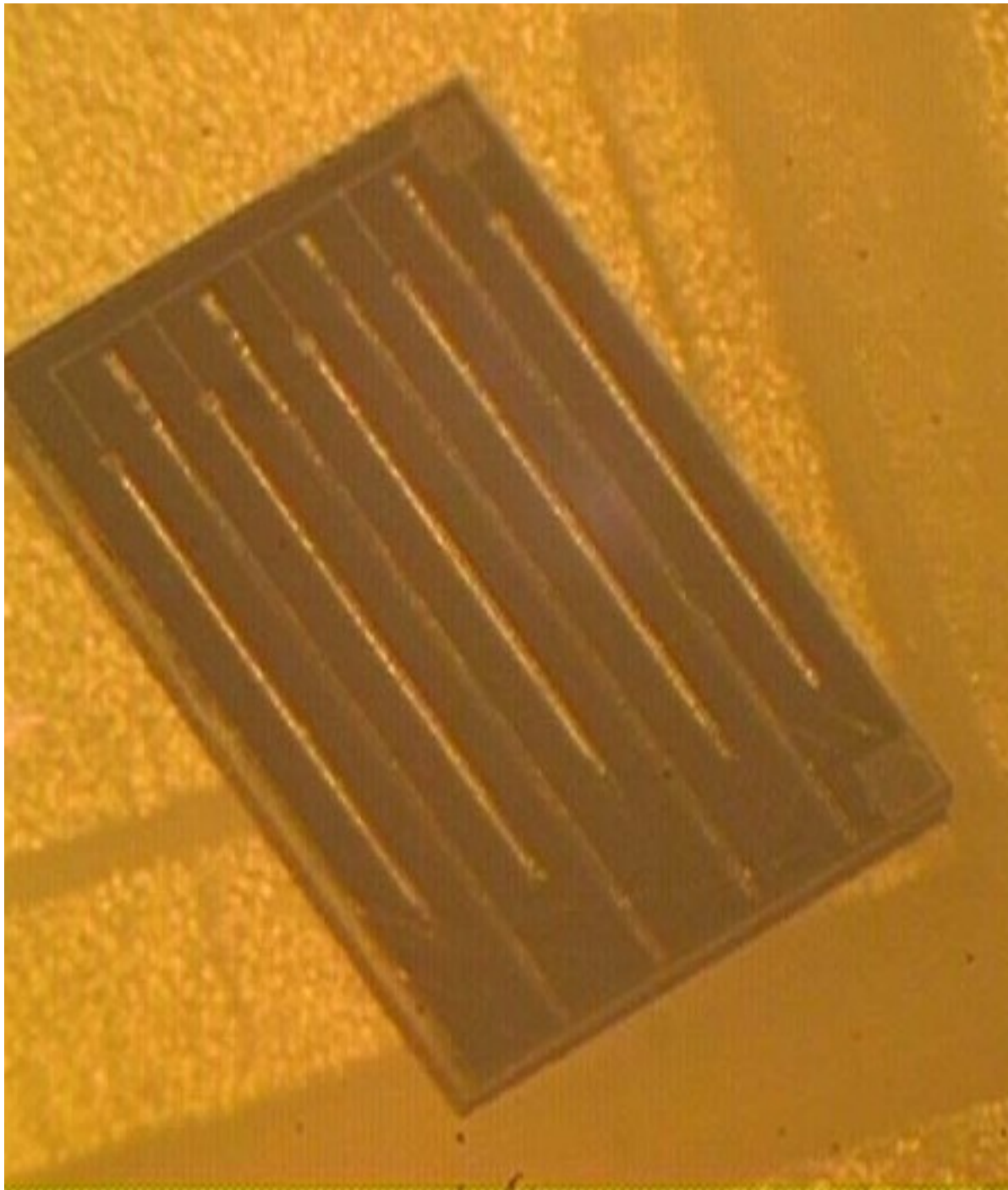
- high average field / peak field,
- a uniform Ramo weighting field,
- an initial pulse time that is independent of the track position and,
- for two facing 100 μm gaps with a common electrode and a 250 μm thickness (in the track direction) a capacitance of 0.527 pF per mm of height.
- For moderate to high bias voltage levels ($\sim 50 \text{ V}$) and low dopant levels ($\sim 5 \times 10^{11} / \text{cm}^3$) we can neglect $V_{\text{depletion}} \approx 2 \text{ V}$, and assume a constant charge-carrier drift velocity. After irradiation, drift velocities will not be uniform, but will be faster as we raise the bias voltage.



Schematic, idealized diagram of induced currents from tracks in a parallel-plate trench-electrode sensor.

Tracks (●) are perpendicular, at the mid and quarter points.

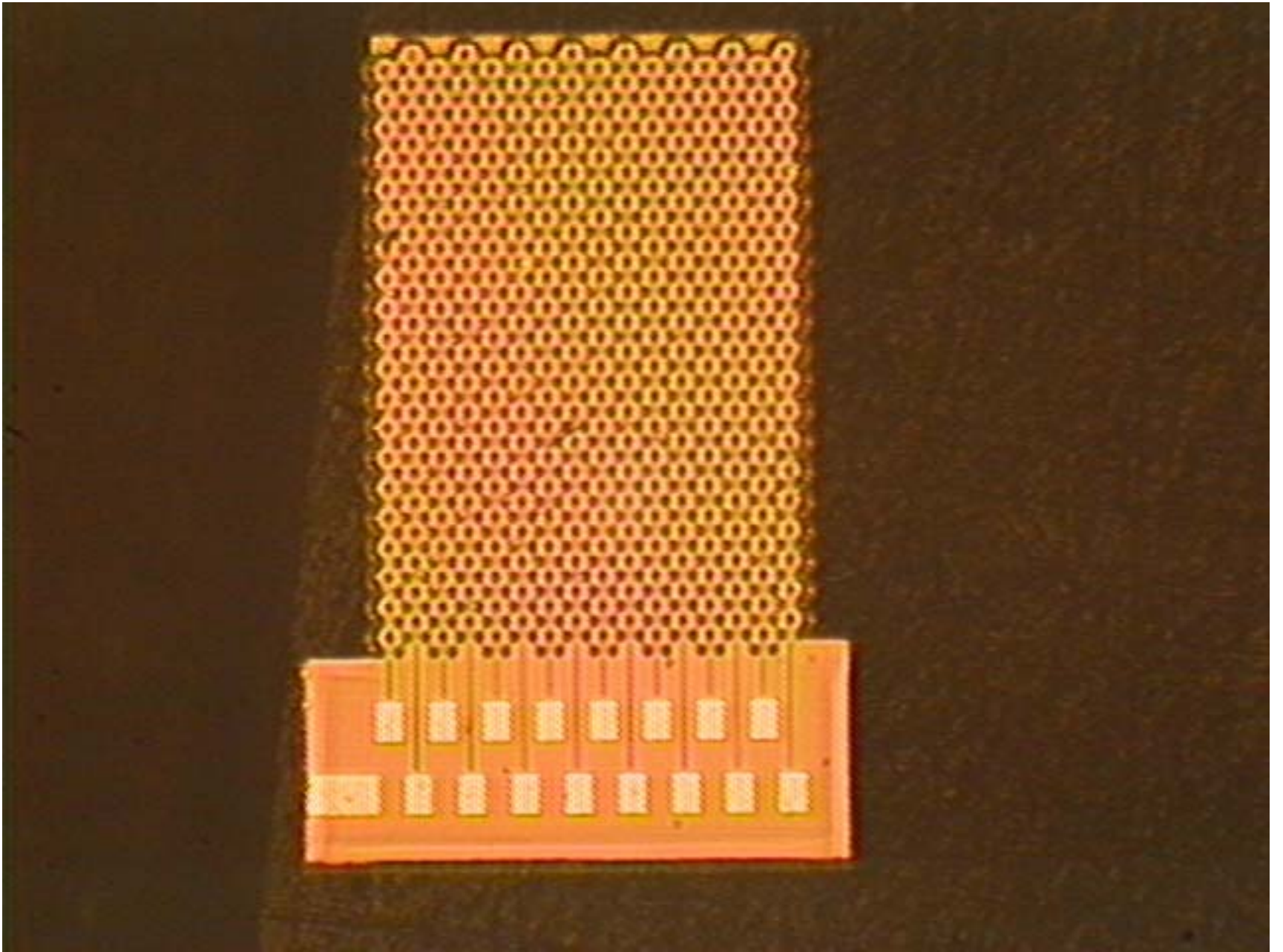
Velocity (electrons) \equiv 3.0 \times Velocity (holes).

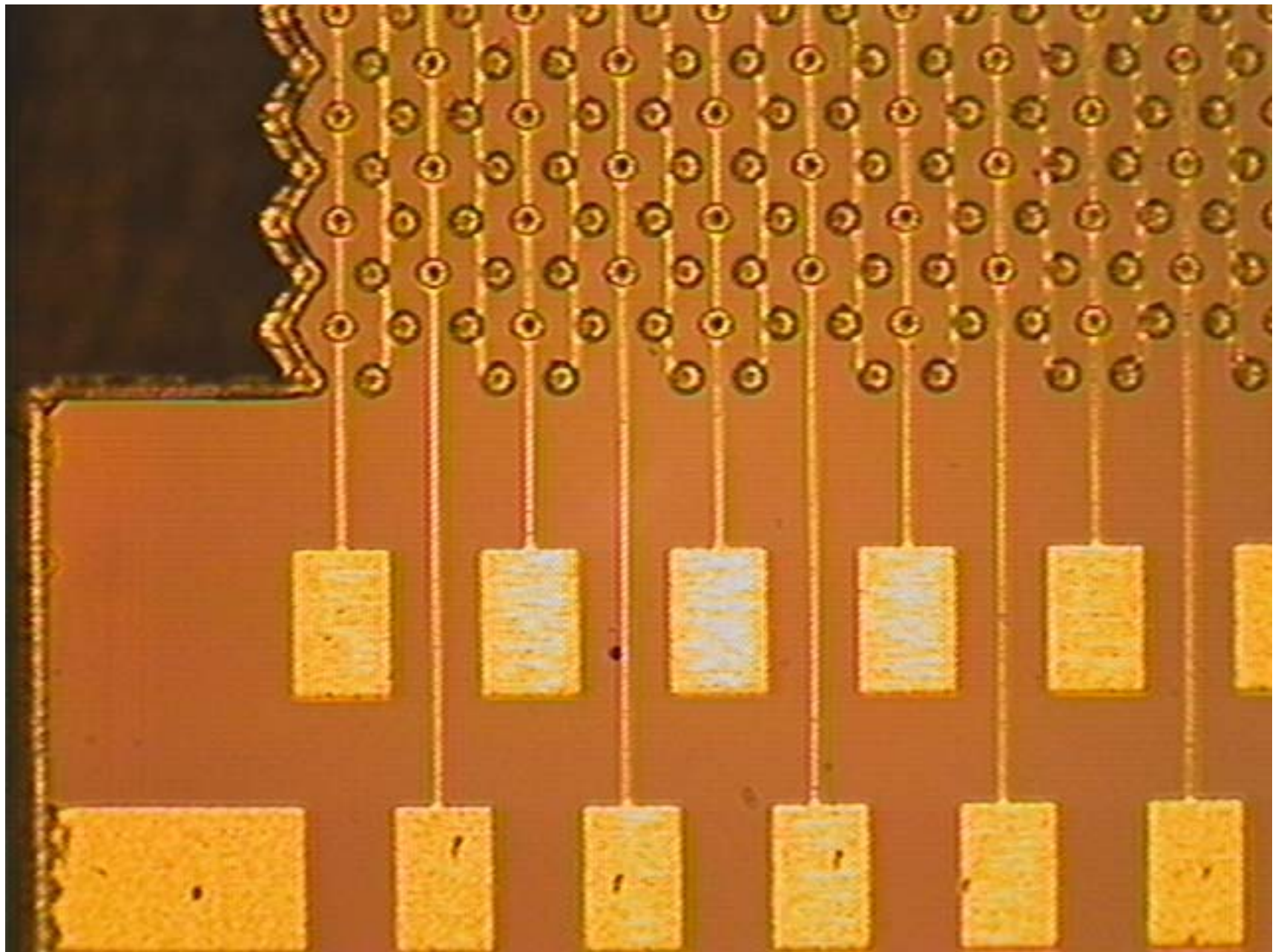


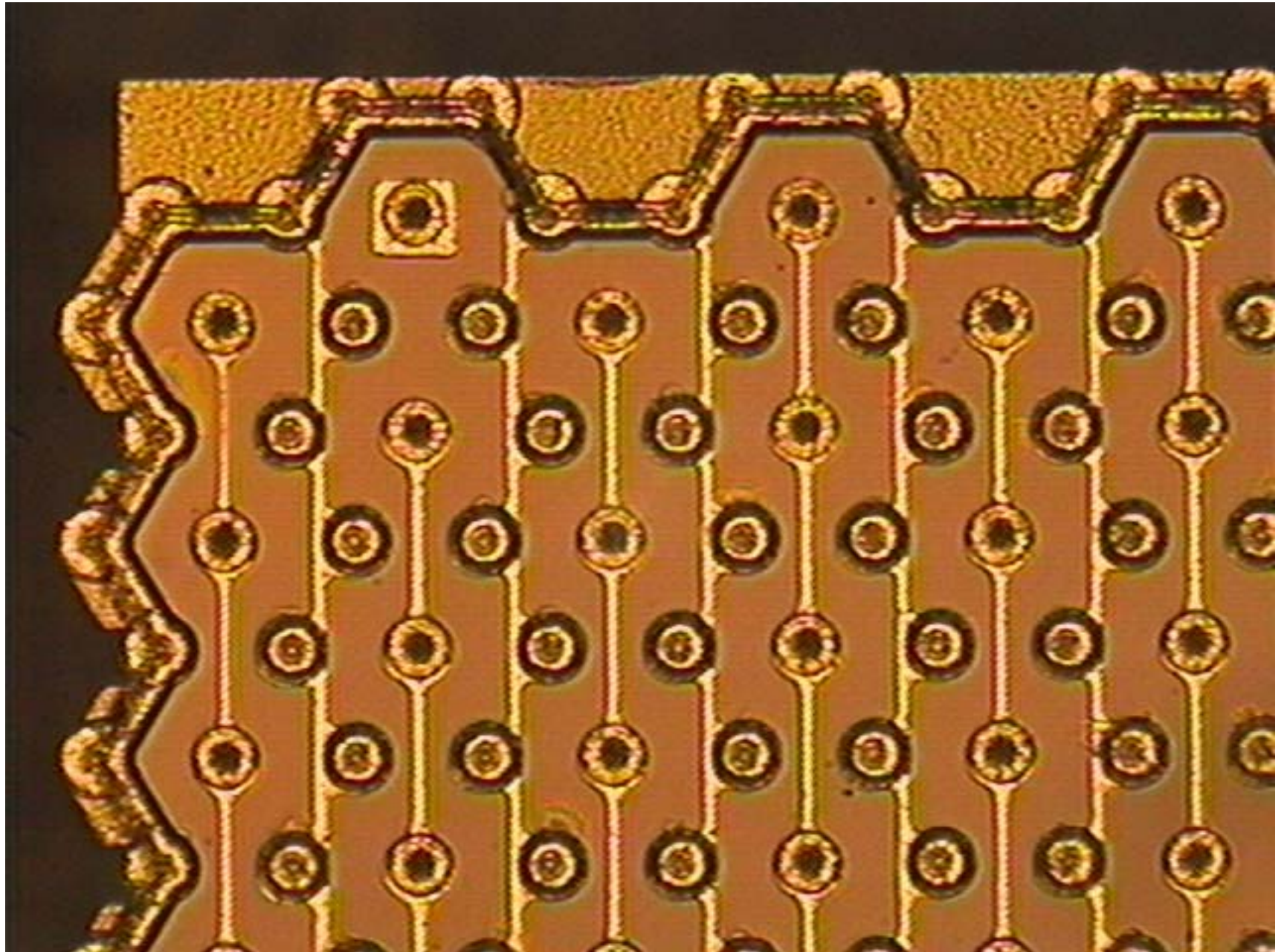
- 1. introduction**
- 2. history**
- 3. factors affecting speed**
- 4. generating the signal – Ramo's theorem**
- 5. amplifying the signal – charge and current amplifiers**
- 6. trench electrode sensors**
- 7. hex-cell sensors**
- 8. experimental results**
- 9. analysis – constant fraction discrimination**
- 10. analysis – fitting with almost-noise-free pulses**
- 11. next**

But for now we used a 50 μm -side hex sensor (following slides)

- 1. with 20 V bias, at room temperature - 40V should be ok,**
- 2. with each column of hexagons tied to a 0.13 μm current-amplifier channel (so large capacitance),**
- 3. exposed to an uncollimated ^{90}Sr beta source,**
- 4. output to an oscilloscope triggered by the signal itself.**





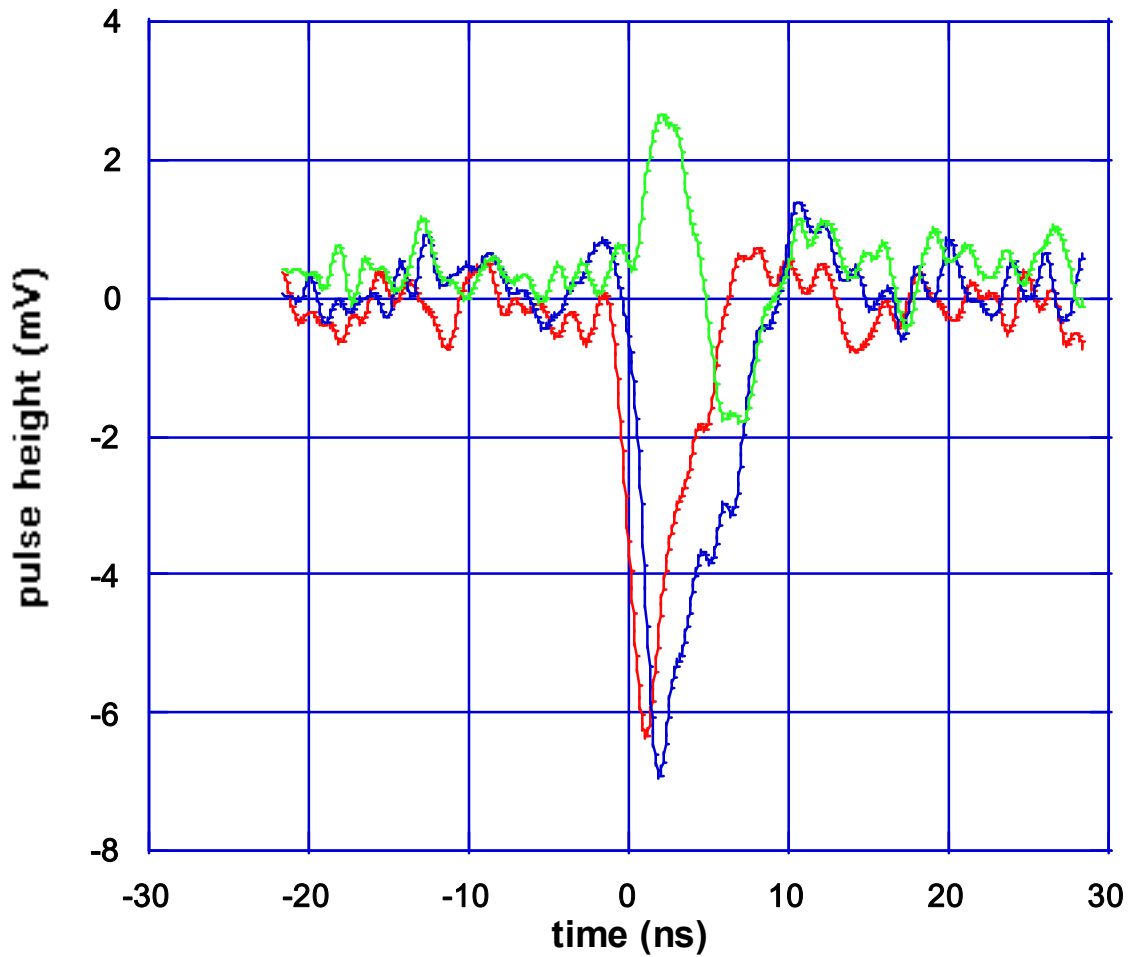


1. **introduction**
2. **history**
3. **factors affecting speed**
4. **generating the signal – Ramo's theorem**
5. **amplifying the signal – charge and current amplifiers**
6. **trench electrode sensors**
7. **hex-cell sensors**
8. **experimental results**
9. **analysis – constant fraction discrimination**
10. **analysis – fitting with almost-noise-free pulses**
11. **next**



a track in two and an induced pulse in the other (green) neighbor

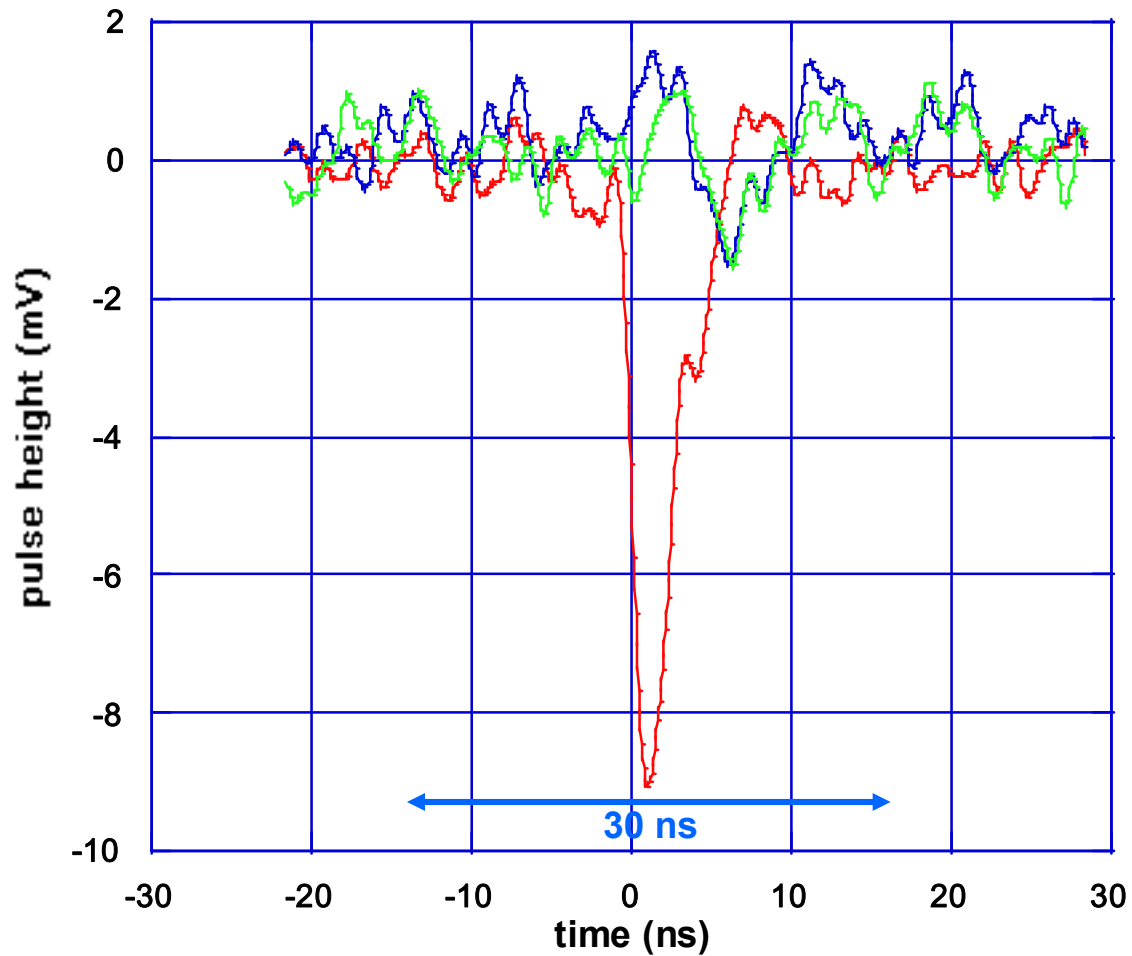
3d.speed.20v.09



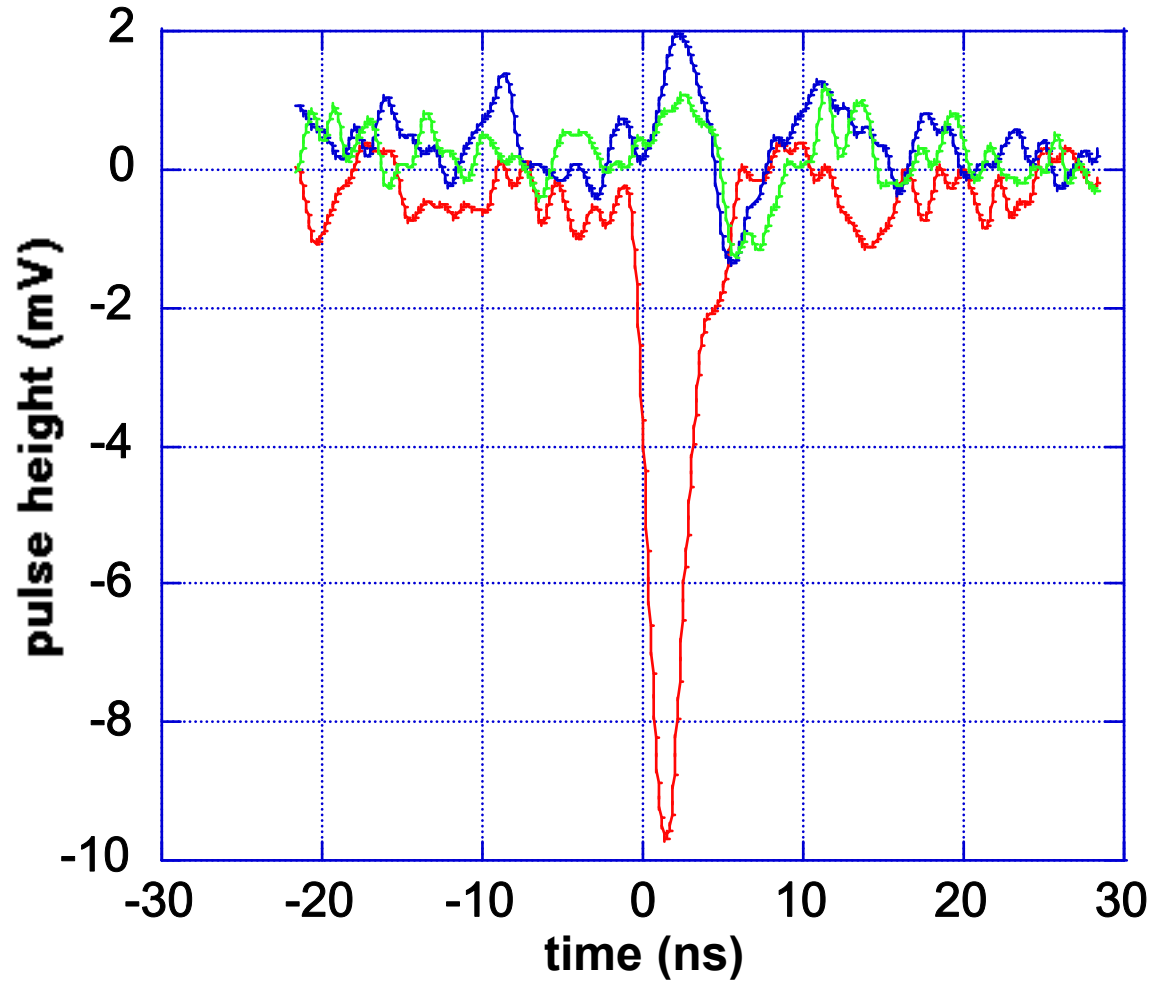
Uncollimated ^{90}Sr betas, 20 C,
hex sensor (20V bias) to 0.13 μm
current amplifier, self-triggers,
event 1 of 99



3d.speed.20v.01



3d.20v.51

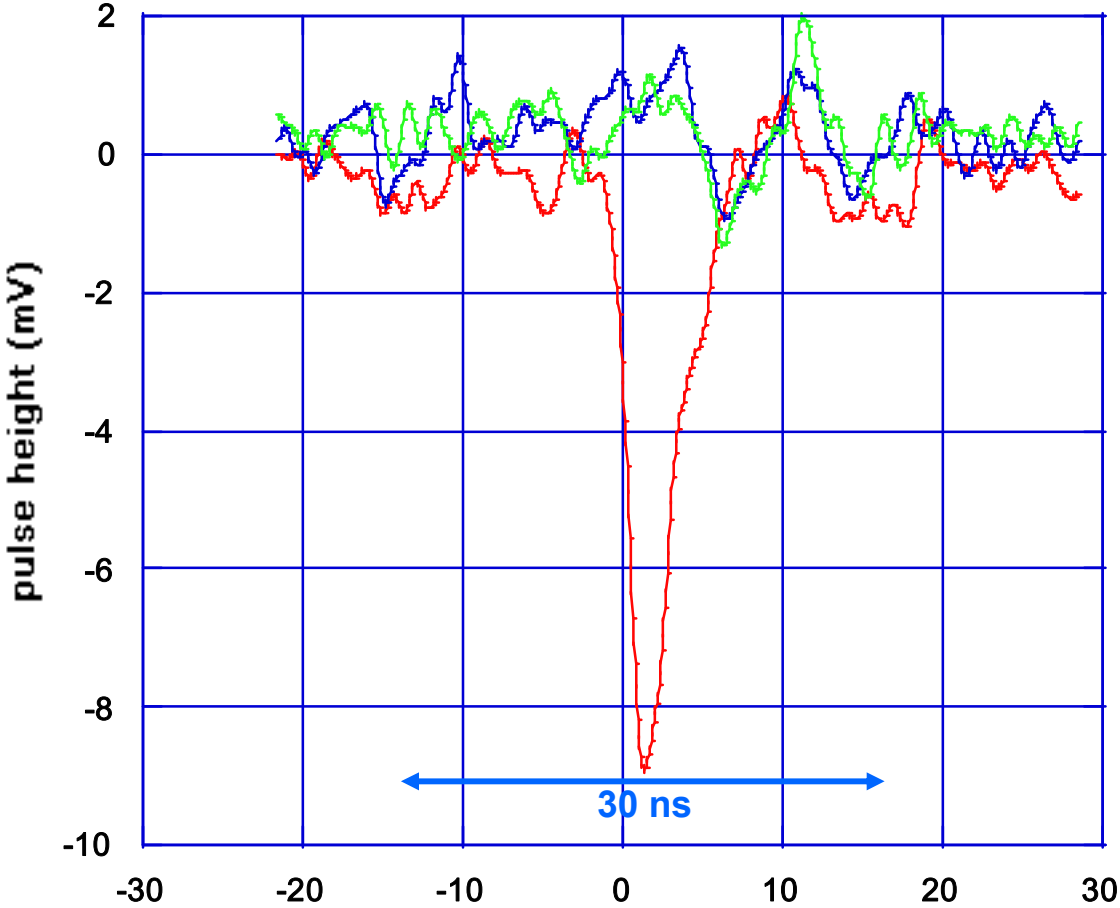


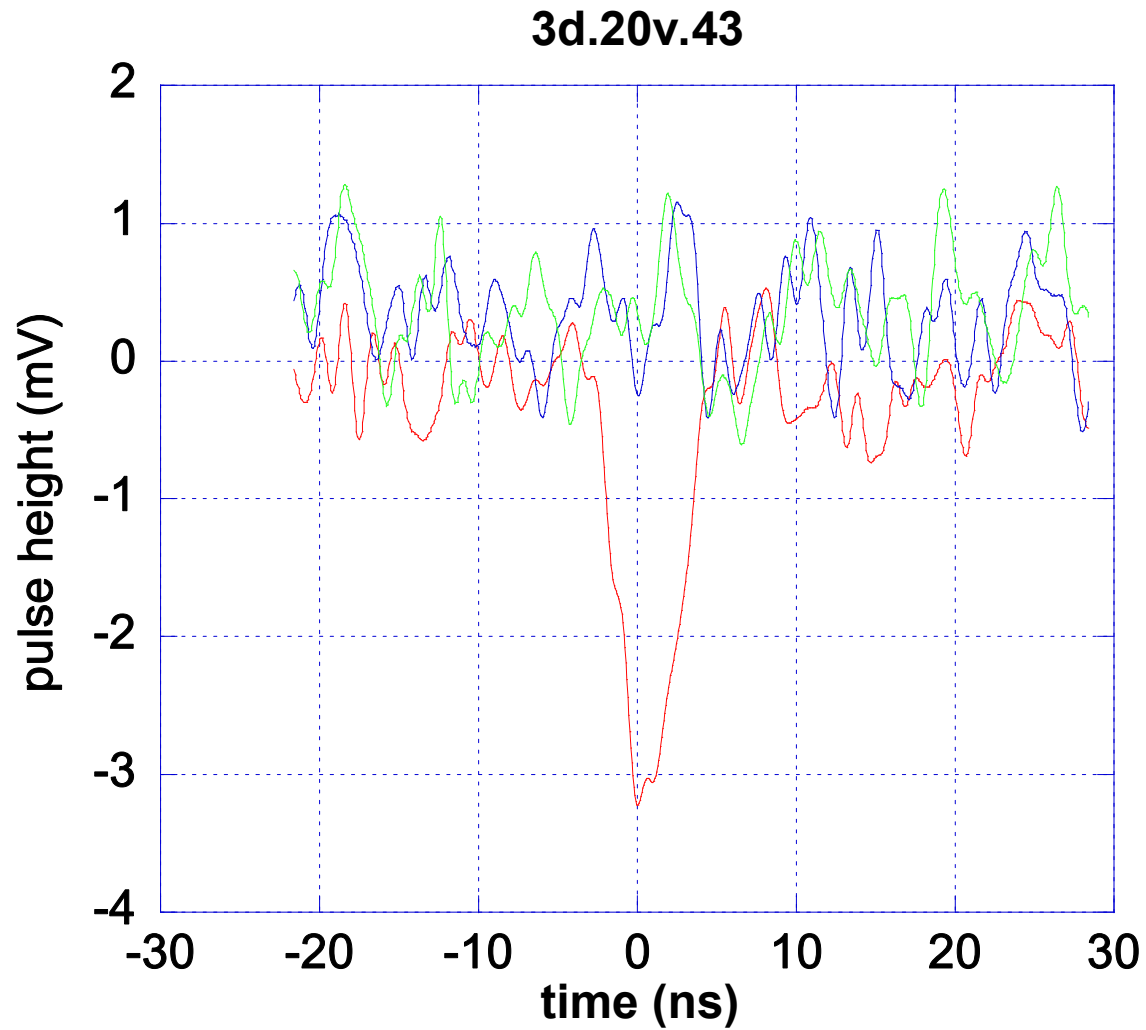
The middle event



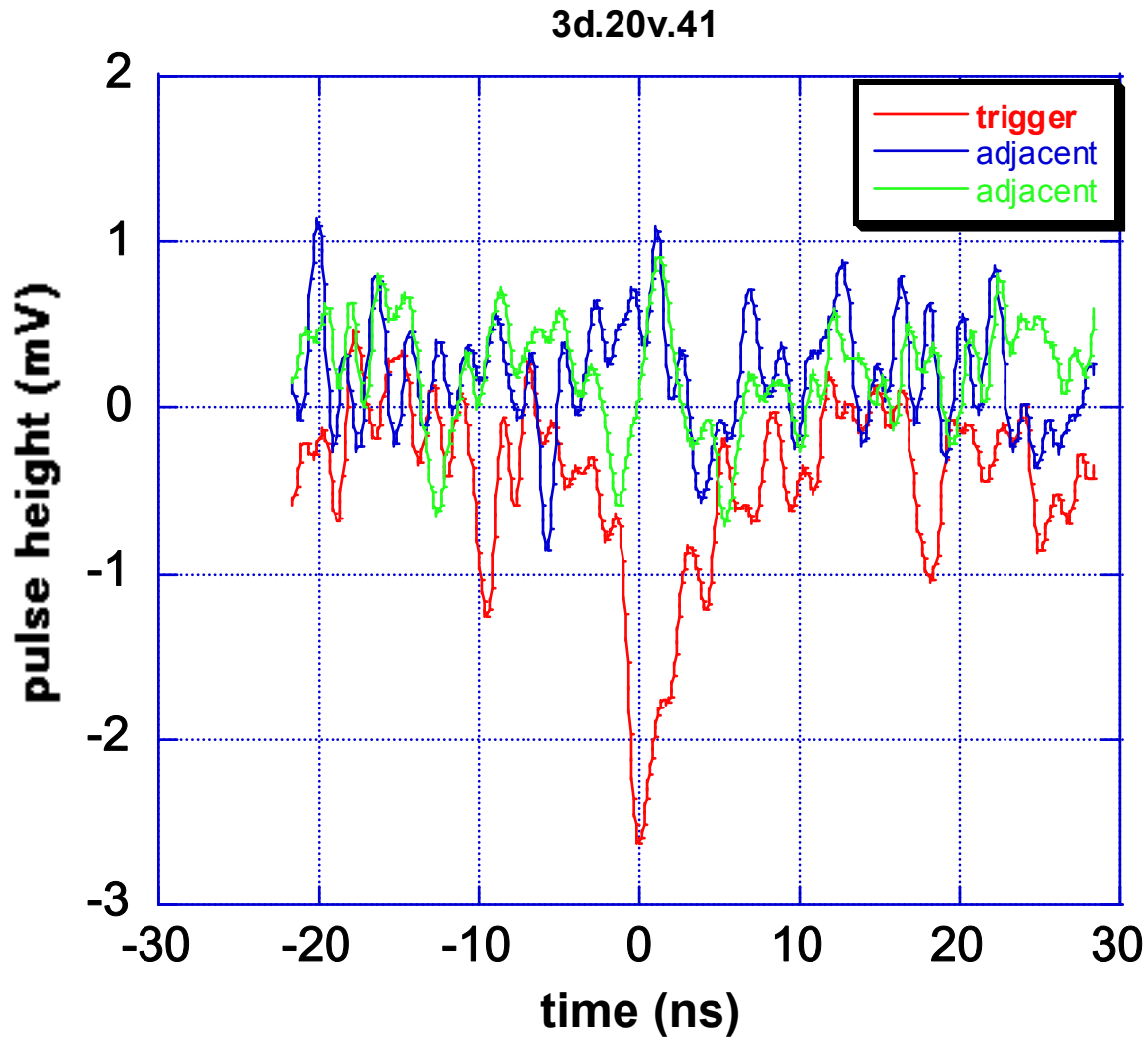
Uncollimated ^{90}Sr betas, 20 C,
hex sensor (20V bias) to 0.13 μm
current amplifier, self-triggers,
event 99 of 99

3d.speed.20v.100





The single-column event with the largest expected timing error in the central scatter plot.

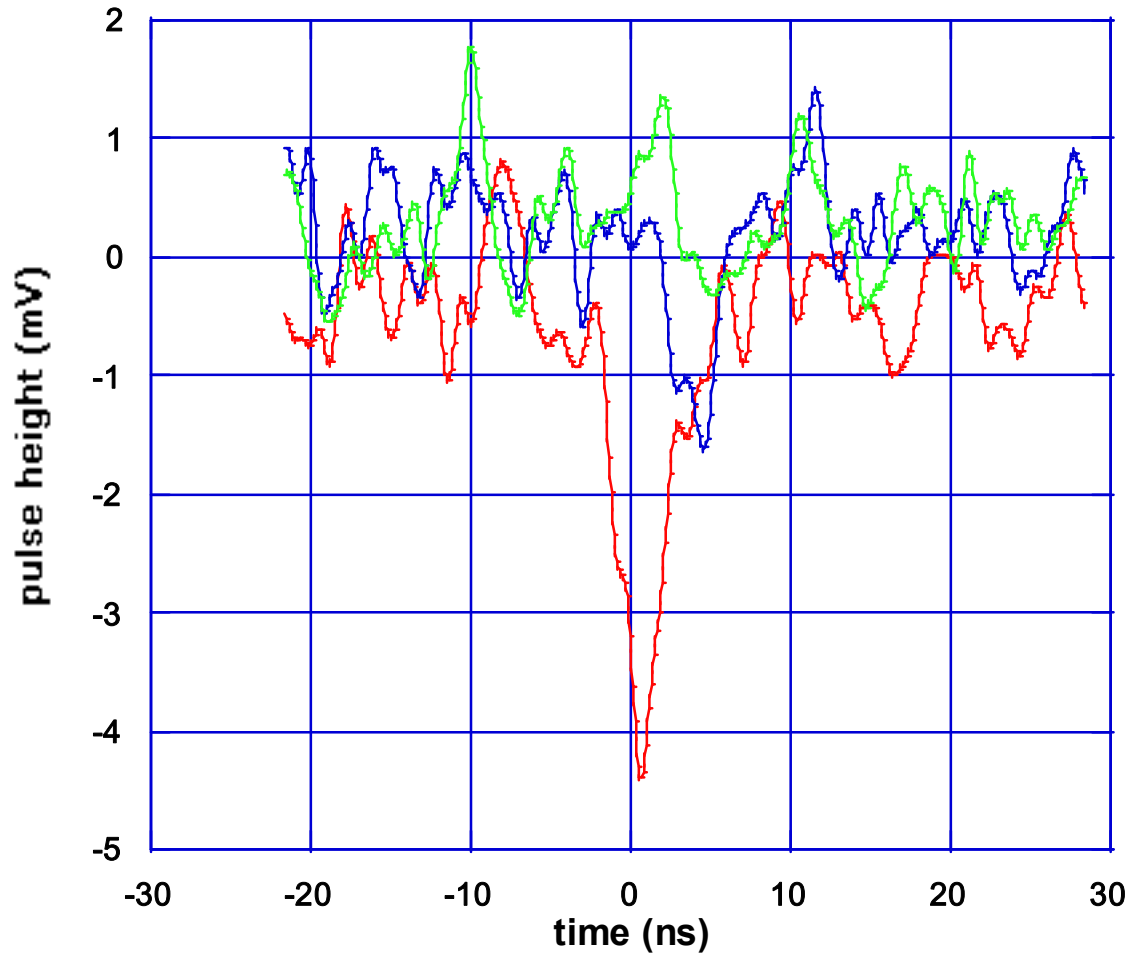


The single-column event with the lowest peak amplitude.

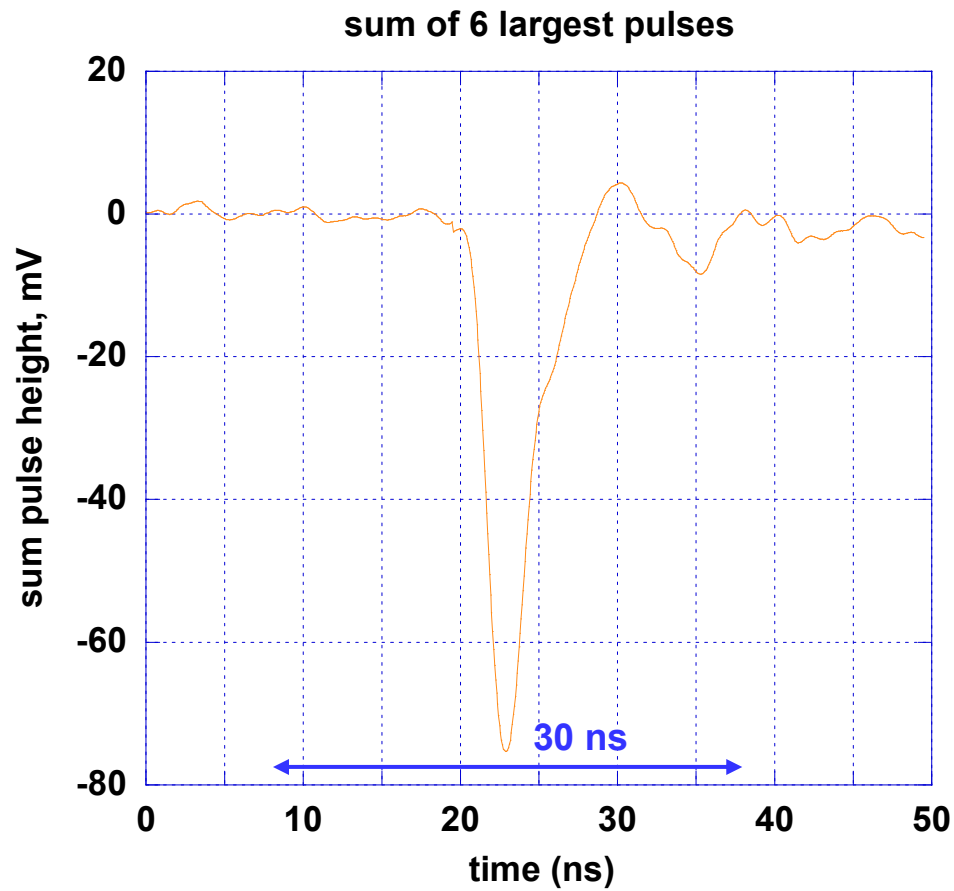
First, one problem with betas: an example of a possible angled track distorting the pulse shape.
(We will need real test beam data)

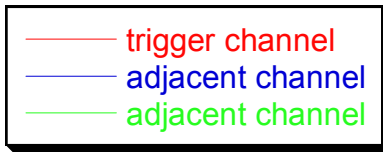


3d.speed.20v.02

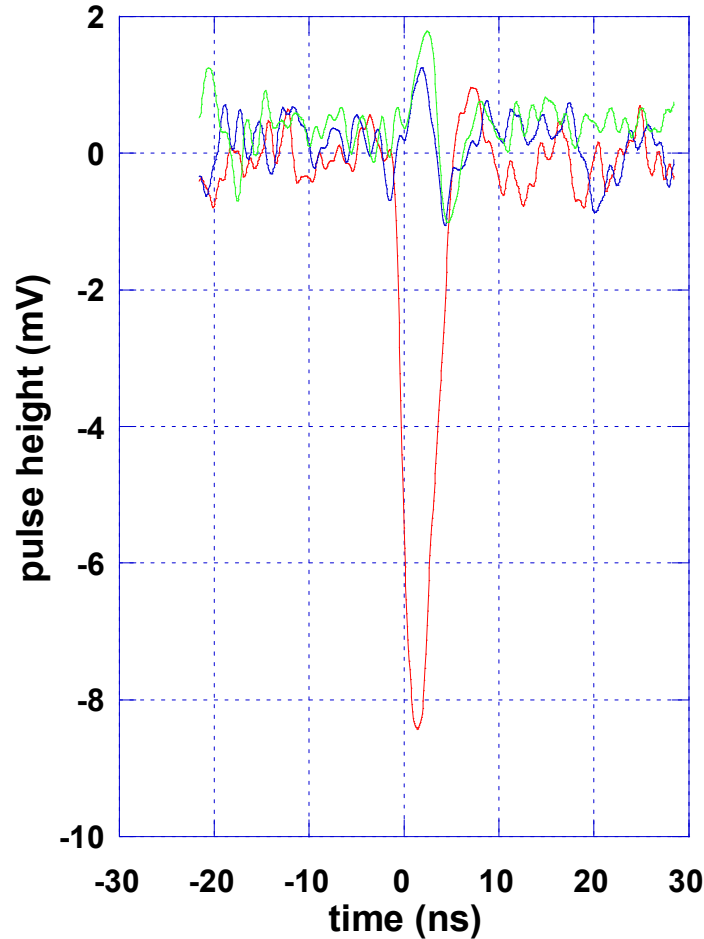


**Pulse shape from the sum of the 6 largest pulses.
 τ -rise = 1.6 ns, fwhm = 2.90 ns. Note the trailing edge
hole current, and amplifier ringing.**



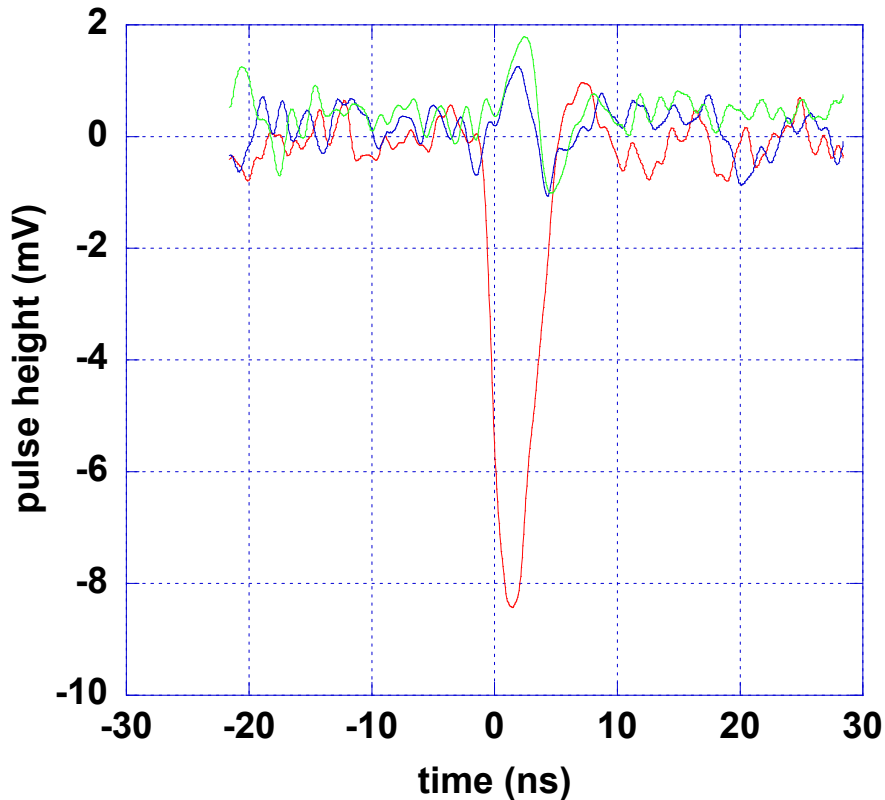


0.8 ns rise time pulse to cal. input

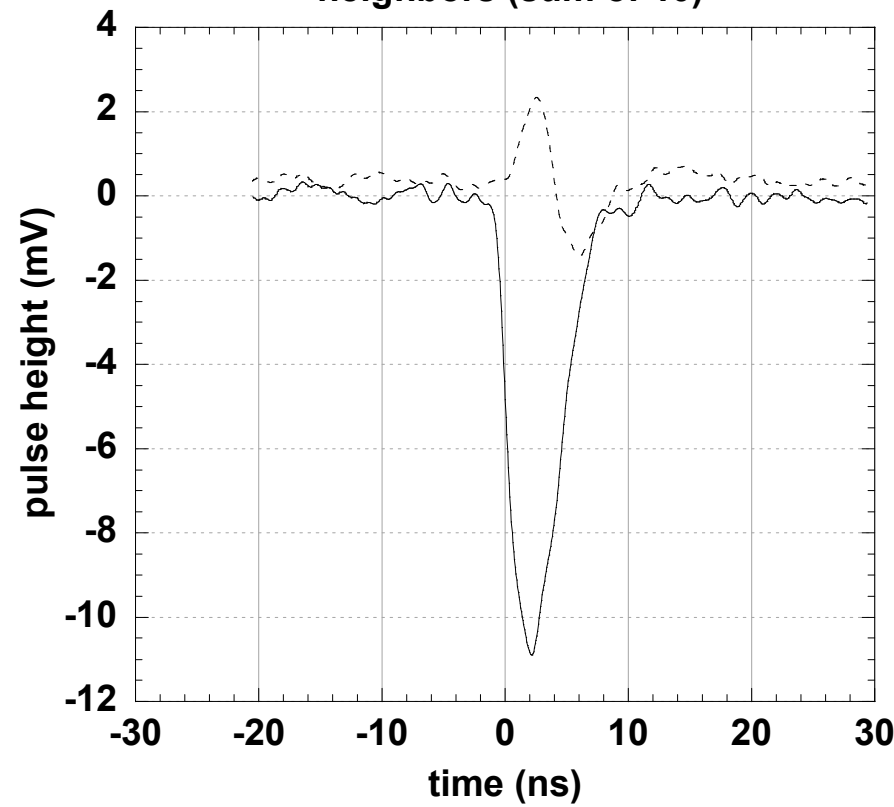


With a pulse from a pulse generator, with the 10% and 90% time points only 0.8 ns apart, we see an amplifier rise time of 1.5 ns. Sensor signals have rise times of 1.6 ns. So the amplifier is currently the limiting element.

0.8 ns rise-time pulse, calibrate input



Pulse generator (sum of 5), neighbors (sum of 10)

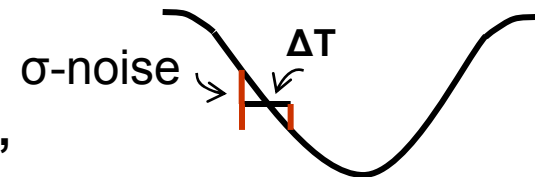


Pulses from an 800 ps rise-time pulse generator with the 2 neighboring channels (left), and the sum of 5 such pulses together with the sum of all 10 neighbor-channel pulses (right). The approximately noise-free shape shows no bulge on the trailing edge, indicating again the tail on the sensor pulses is not electronic in origin, but rather due to hole motion. It can also be seen that the signals in the neighboring channels are induced and that the noise is reduced.

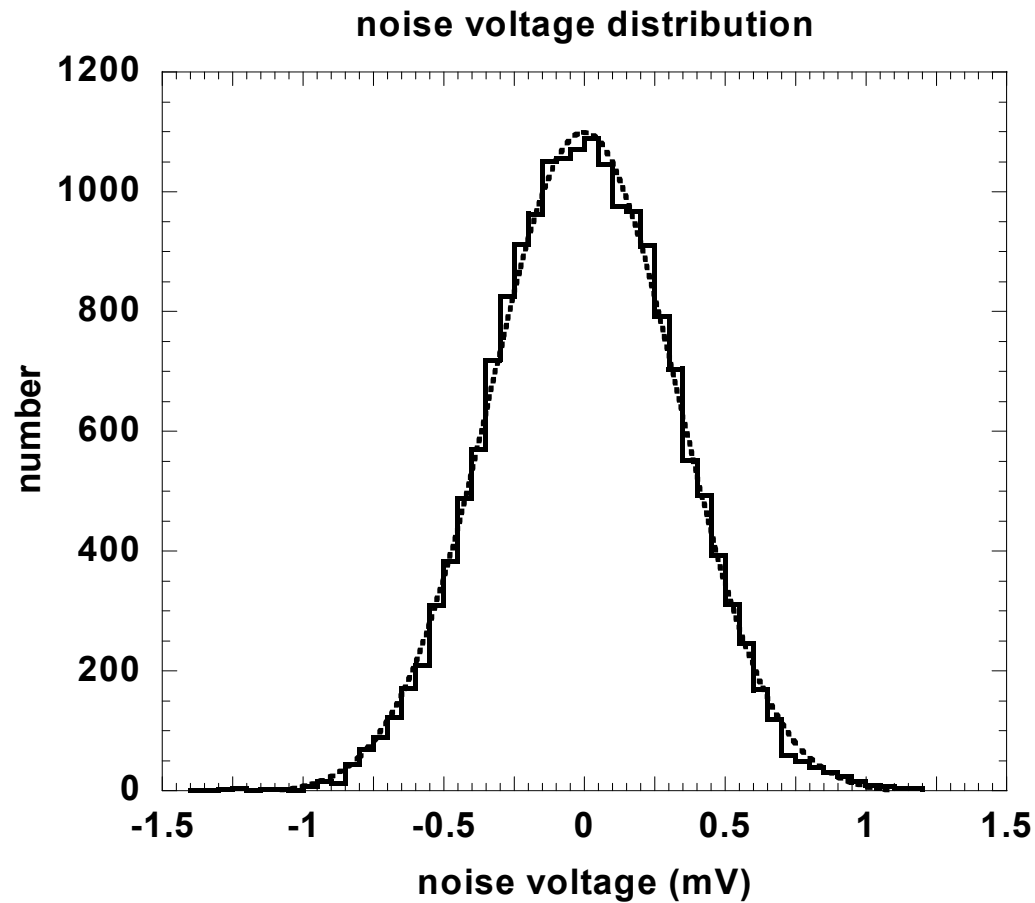
- 1. introduction**
- 2. history**
- 3. factors affecting speed**
- 4. generating the signal – Ramo's theorem**
- 5. amplifying the signal – charge and current amplifiers**
- 6. trench electrode sensors**
- 7. hex-cell sensors**
- 8. experimental results**
- 9. analysis – constant fraction discrimination**
- 10. analysis – fitting with almost-noise-free pulses**
- 11. next**

Estimate the time resolution at room temperature with

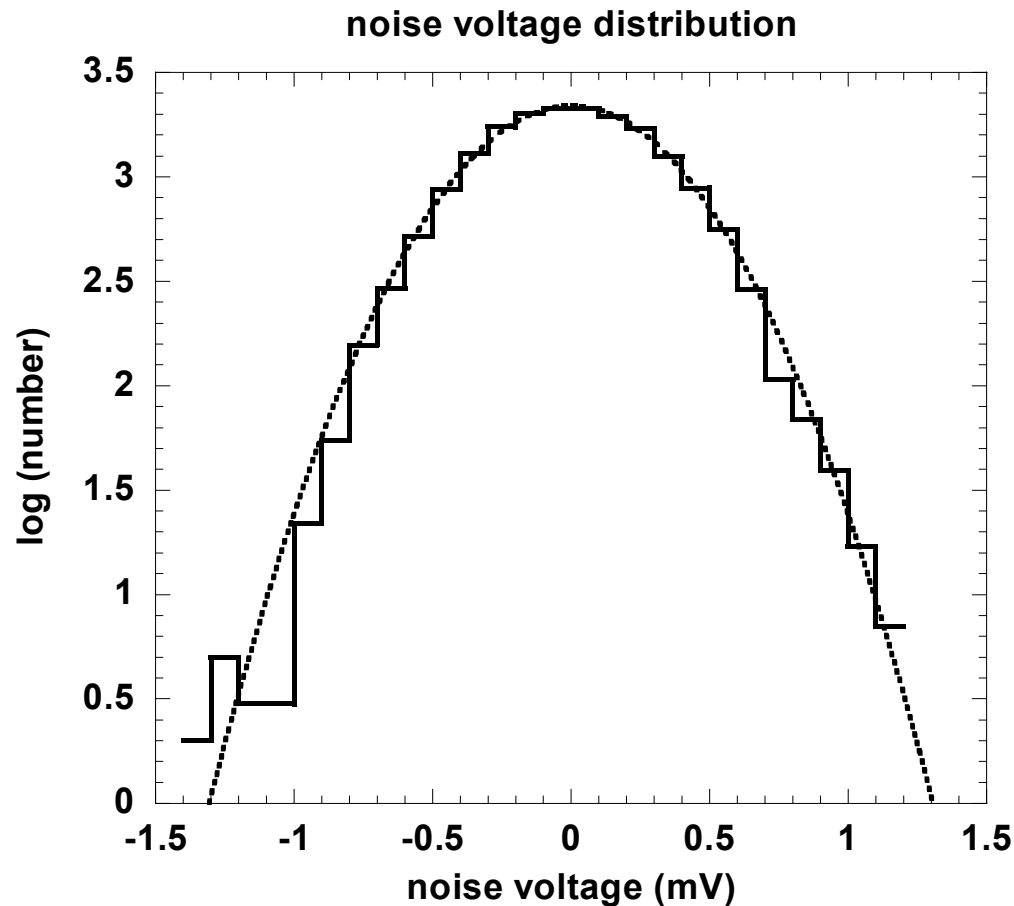
- the hex sensor, and
- a preliminary version of a $0.13\ \mu\text{m}$ integrated circuit readout
- using data from un-collimated 90-Sr β s (but only with tracks in the central channel).
- (A wall-electrode with parallel plates would give shorter times, but the hex sensor already has almost the same output rise time as a $0.8\ \text{ns}$ input rise time pulse generator, so the output shape is primarily determined by the amplifier, not the sensor).
- To simulate a constant fraction discriminator set at 50% (where slope is steepest):
 - Fit leading baseline, and measure noise,
 - Fit top and find halfway point,
 - $\Delta T = \sigma\text{-noise} / \text{slope}$
 - With wall-electrode sensor and a parallel beam,
 - can do better fitting entire pulse.



Noise distribution from pre-pulse region with a Gaussian fit.



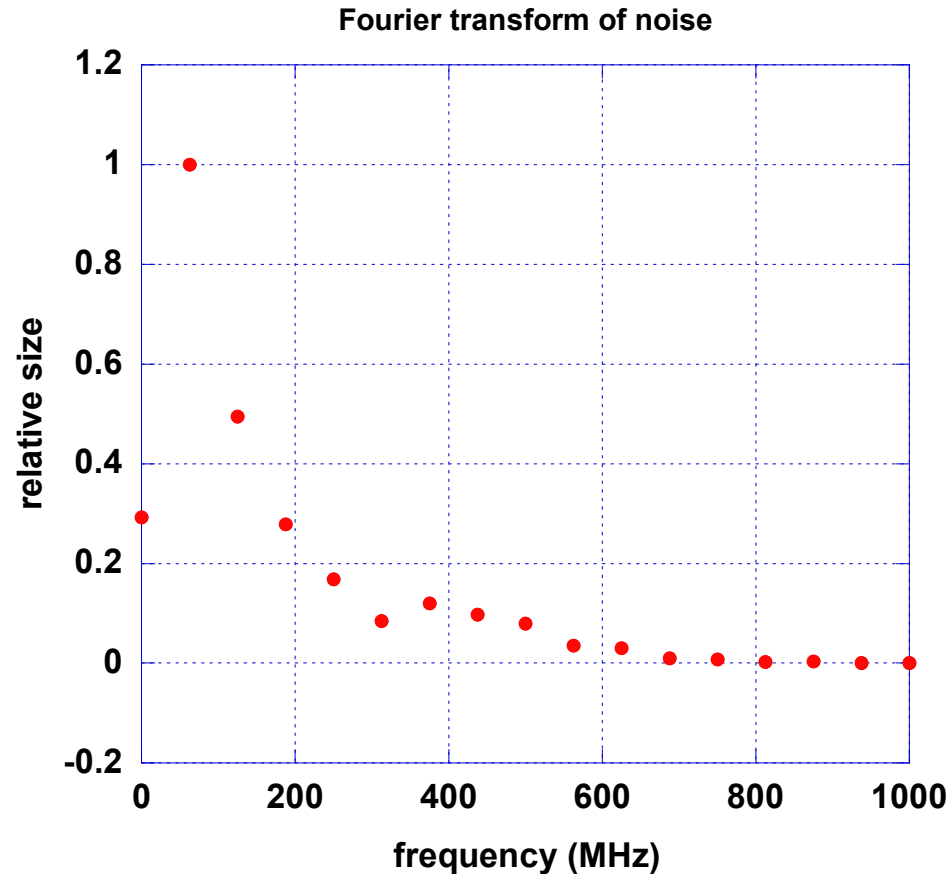
Noise distribution from pre-pulse with a Gaussian fit – log scale to show tails

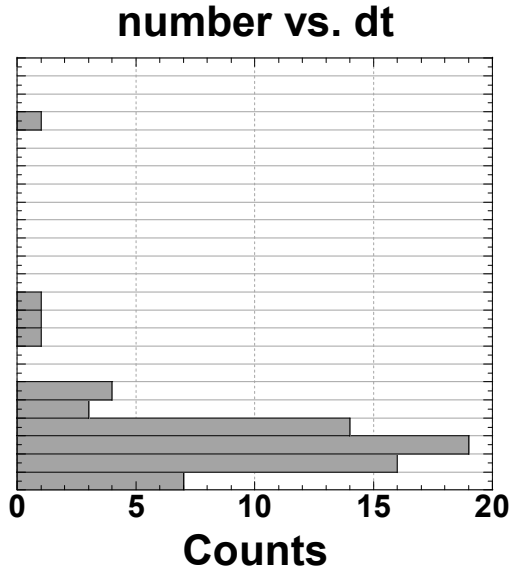
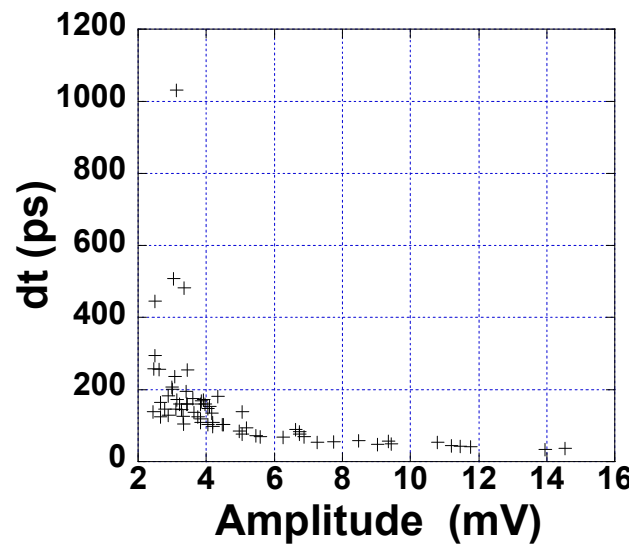
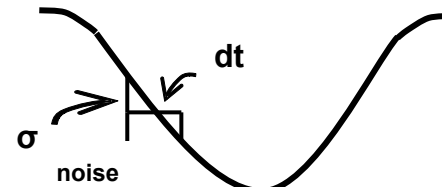
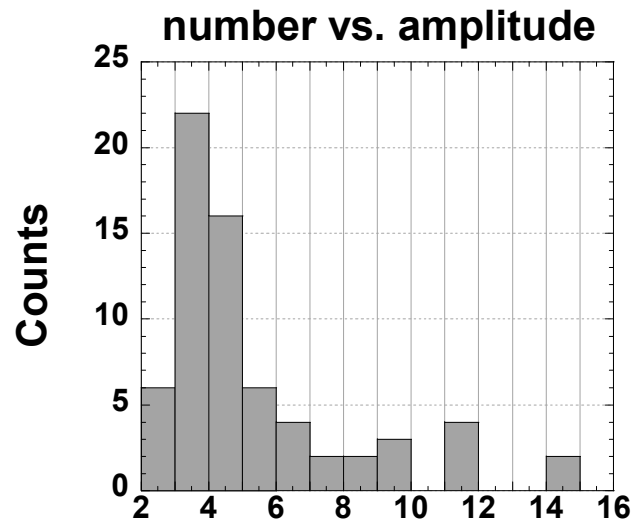


sigma = 0.33166 +/- 0.0033 mV

direct standard deviation from the 18,090 voltage values = 0.3218 mV

Fourier transform of noise: Gaussian, but not white





Scatter plot of expected noise-induced timing errors, dt , vs. pulse amplitude, for 67 pulses and the projections of dt and amplitude distributions. σ (noise) = 0.33 mV.

- 1. introduction**
- 2. history**
- 3. factors affecting speed**
- 4. generating the signal – Ramo's theorem**
- 5. amplifying the signal – charge and current amplifiers**
- 6. trench electrode sensors**
- 7. hex-cell sensors**
- 8. experimental results**
- 9. analysis – constant fraction discrimination**
- 10. analysis – fitting with almost-noise-free pulses**
- 11. next**

1. An approximately noise-free signal pulse shape was found by adding the six pulses above 10 mV, which are already relatively noise-free. To allow for the slight trigger-time variations, the individual curves were shifted by amounts of up to ± 0.25 ns to align the peaks.
2. A set of noise sequences was prepared by subtracting the average of each 270-point pre-pulse base line from the 270 points to remove common-mode signals from each of the 67 traces.
3. The 67 baselines were subdivided into $67 \times 3 = 201$ sets of 90 points each, covering $(90 / 16)$ ns a time longer than the pulse-sections used (the rise once above the noise-level, the top, and the first part of the trailing edge.)
4. The stored signal pulse amplitudes were multiplied by a fraction to reduce them to the height of the smallest of the 67 signals.
5. The first noise sequence was added, point-by-point, to the reduced-amplitude signal.

6. The peak of the digital pulse **plus noise** in step 5 above was used to adjust the peak height of the pulse to be fitted, and proportionately, all of the other points. So all of these points will be off by a common but realistic error factor. Since the same function is used for both pulses, errors from track angle variations will not be present, but they will also not be present in the first possible use which would employ high-energy, normally-incident tracks.
7. The fitted track amplitudes were subtracted, point-by-point from the signal plus noise.
8. The standard deviation of these differences was calculated.
9. Steps 7 and 8 were repeated with the fitted set shifted one point (62.5 ps) later.

10. Steps 7–9 were repeated for a total of $(77 - 15) - (65 - 22) = 19$ times.

11. The minimum standard deviation of the 19 was found.

12. A parabola was fit to that minimum value and the two values on each side.

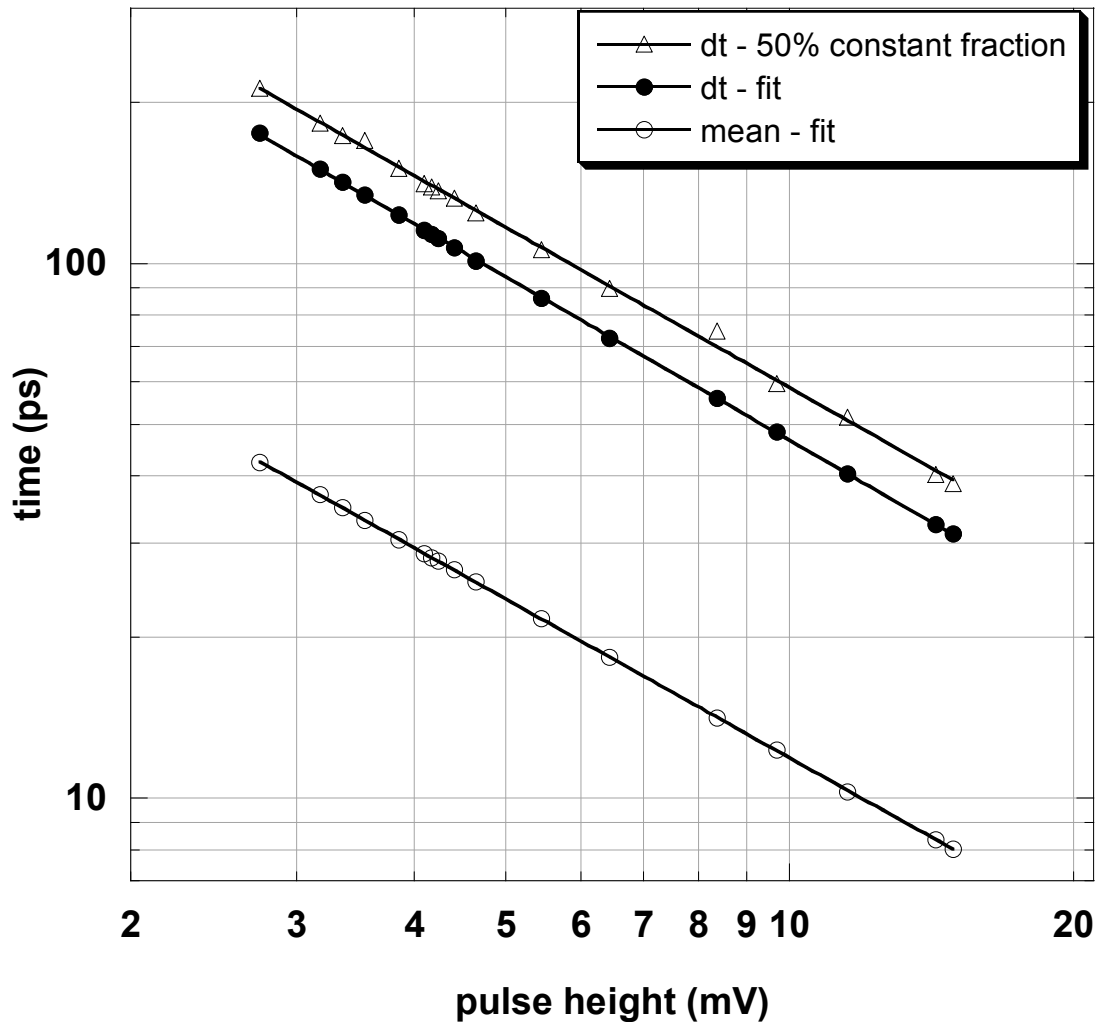
13. The minimum location will be used to interpolate between the steps. A parabola with (x,y) points $-x, 0, x$ and y_1, y_2, y_3 ($x = 62.5$ ps) has a minimum at:

$$x_0 = (x / 2)(y_1 - y_3) / (y_1 - 2 y_2 + y_3)$$

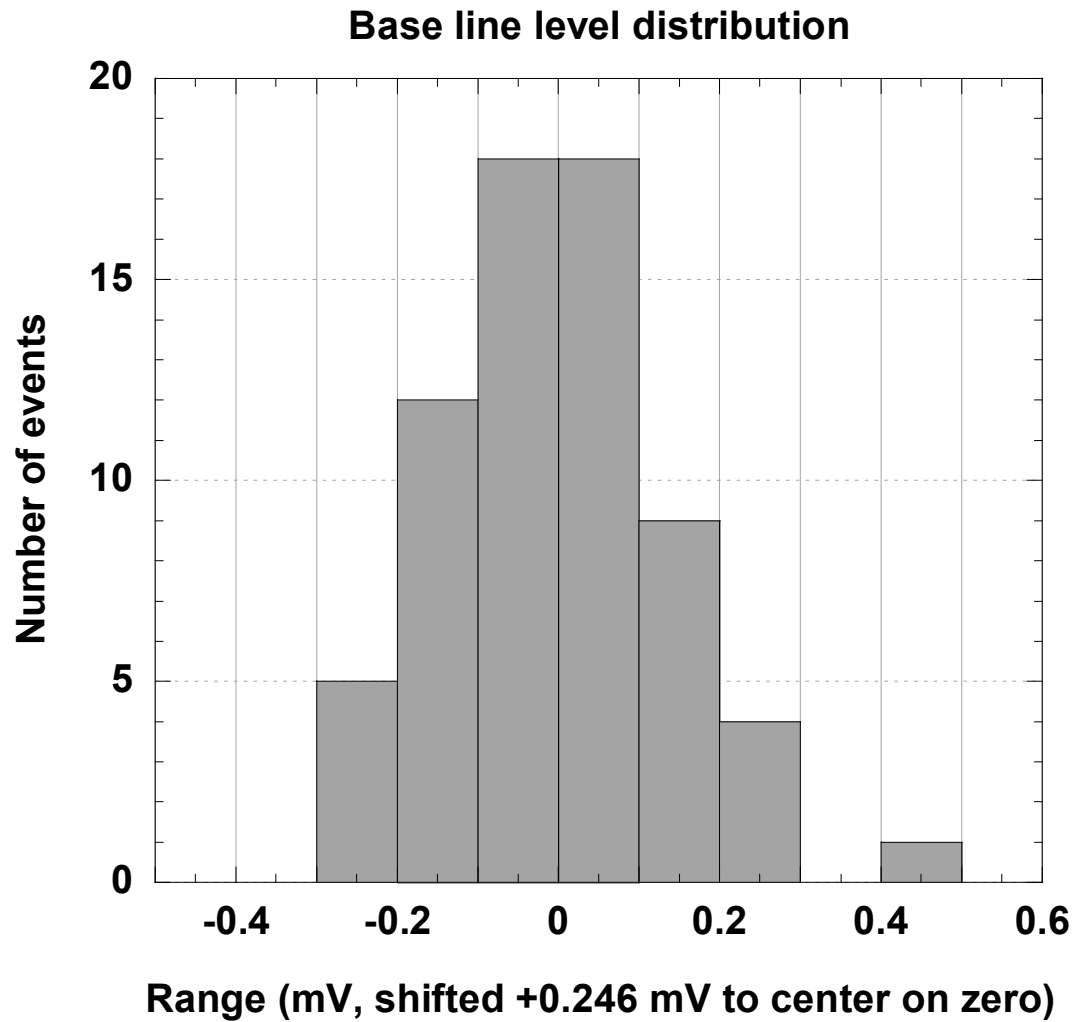
14. The standard deviation of these 201 interpolated parabola minima was found and is plotted in the next slide.

Standard Deviation

$$\sqrt{\frac{\sum_{i=1}^n x_i^2 - n(\bar{x})^2}{n-1}}$$



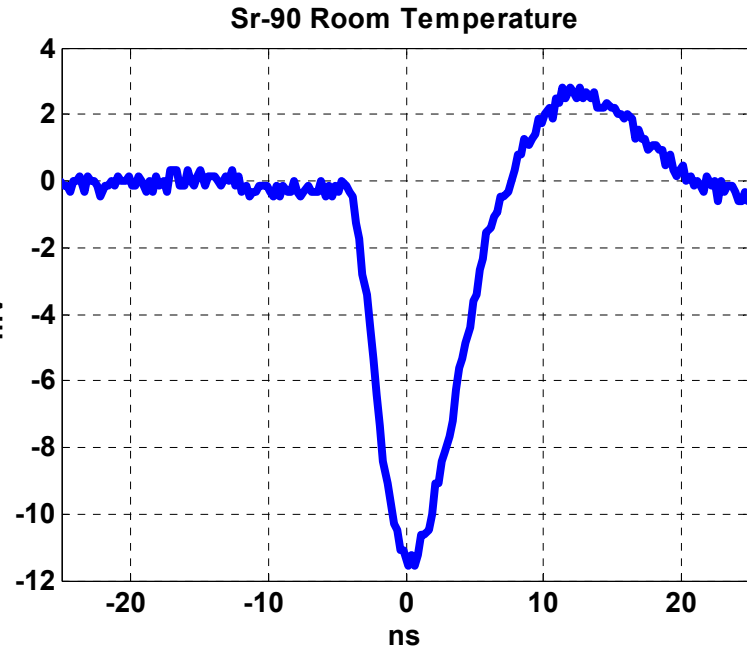
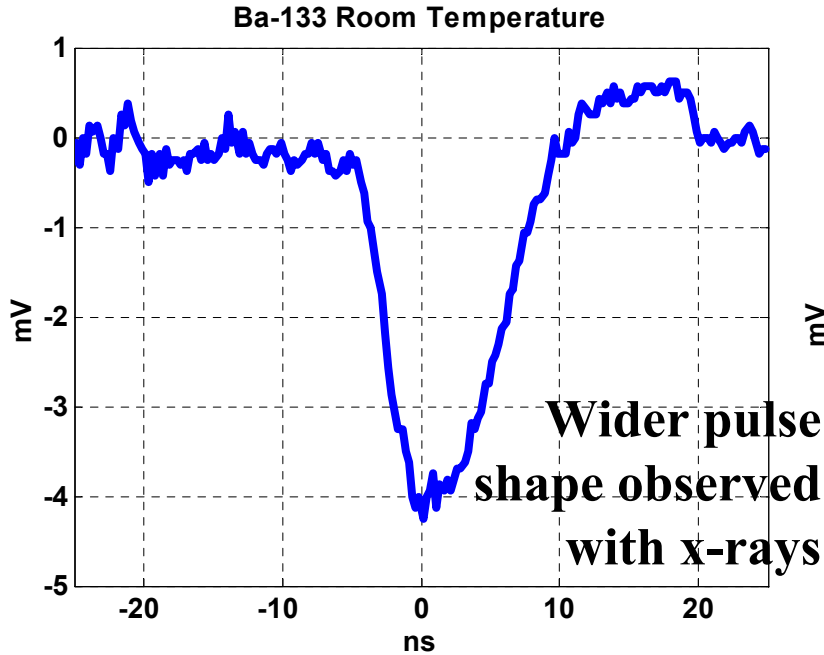
Expected time errors, dt, due to noise as a function of pulse height from the combined signal pulse shape added to 201 noise segments with dt determined from the **standard deviation** of time variation of the 50% point on the leading edge (△) and from the time variation of the best fit time of the combined signal pulse shape to the same shape plus noise (●). The mean value of the best fit times (○) is 24% of the fit values. The signal to noise ratio is 3 times the pulse height in mV.



Base line event-to-event shift distribution. The standard deviation of the 67 events is 0.14 mV.

- 1. introduction**
- 2. history**
- 3. factors affecting speed**
- 4. generating the signal – Ramo's theorem**
- 5. amplifying the signal – charge and current amplifiers**
- 6. trench electrode sensors**
- 7. hex-cell sensors**
- 8. experimental results**
- 9. analysis – constant fraction discrimination**
- 10. analysis – fitting with almost-noise-free pulses**
- 11. next**

Pulses from x-ray & beta (RT)



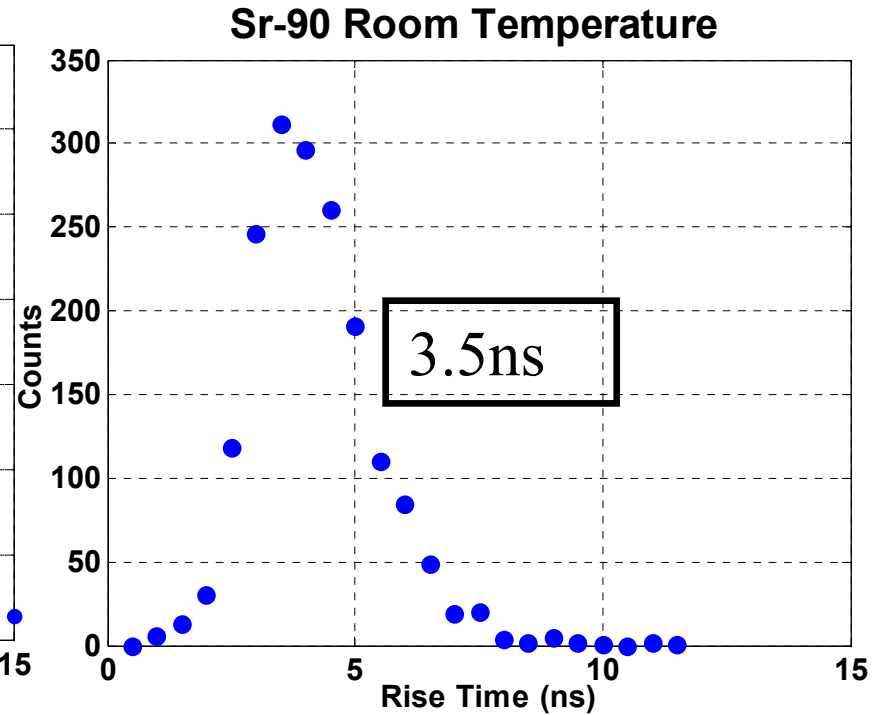
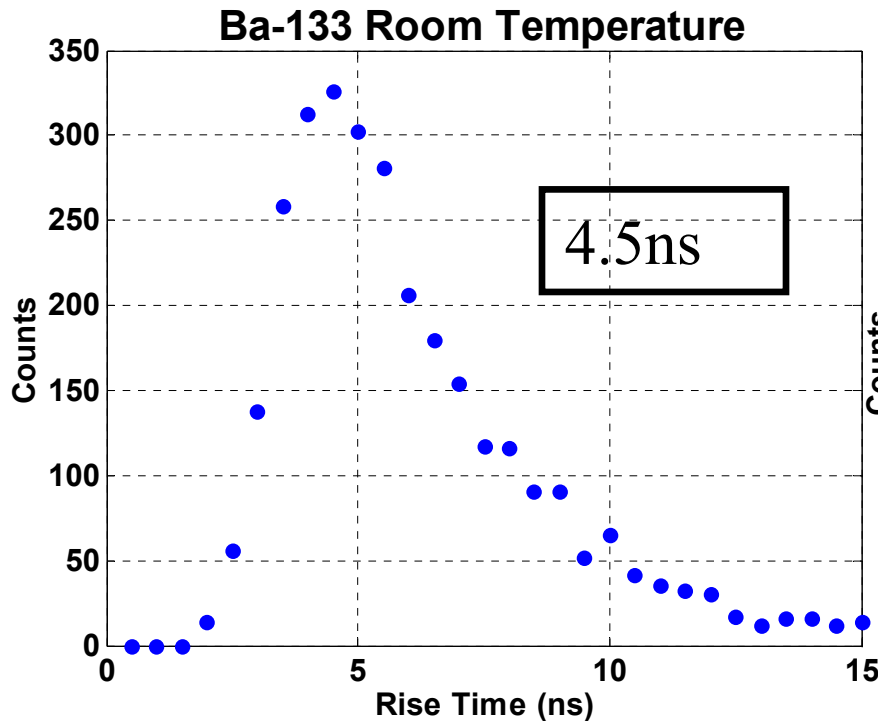
Rise Time (ns)	4.5ns
fwhm (ns)	10.0ns
Fall Time (ns)	5.5

Rise Time (ns)	3.5ns
fwhm (ns)	9.5ns
Fall Time (ns)	4.0

Measurement Results (non-irradiated RT)

Rise Time Distribution

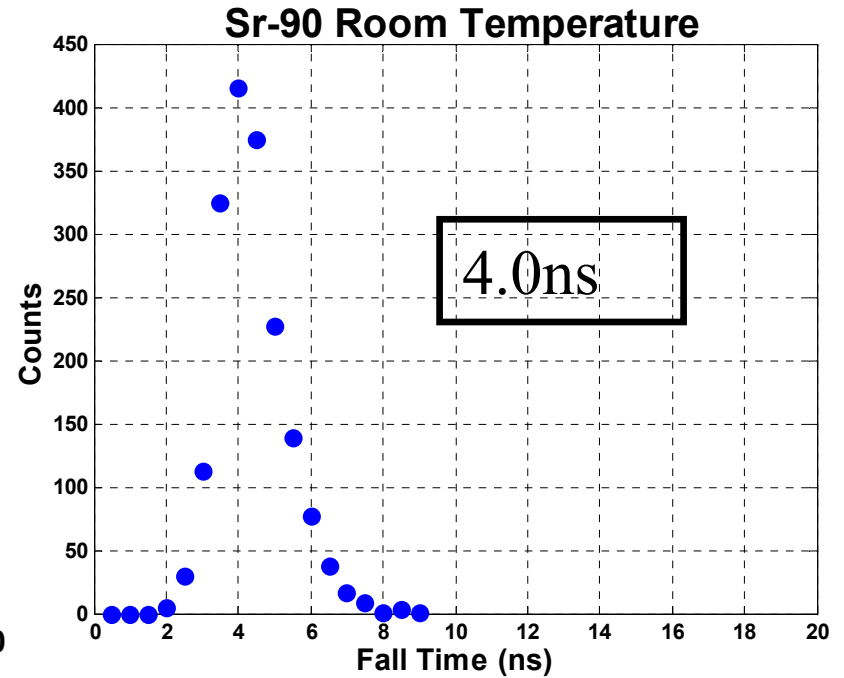
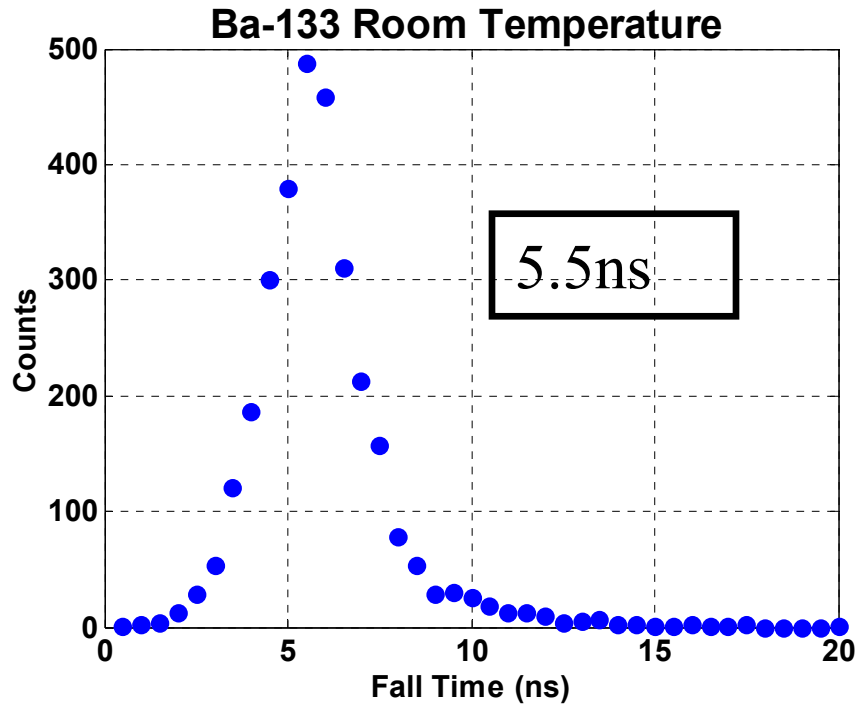
- Faster rise time observed using Beta source (Sr-90)
- Statistics agrees with single pulse observation
 - ❖ Pulses from x-ray are slower



Measurement Results (non-irradiated
RT)

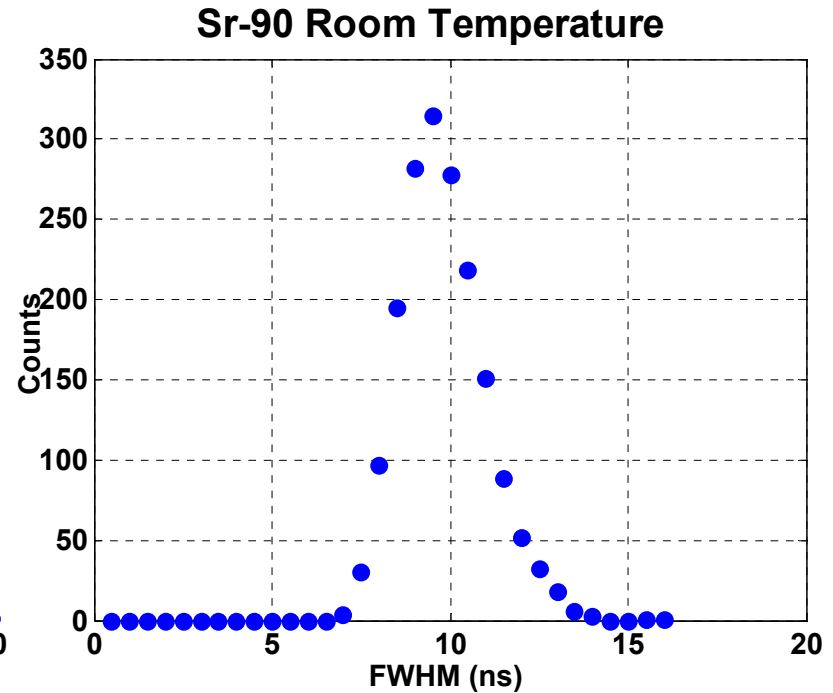
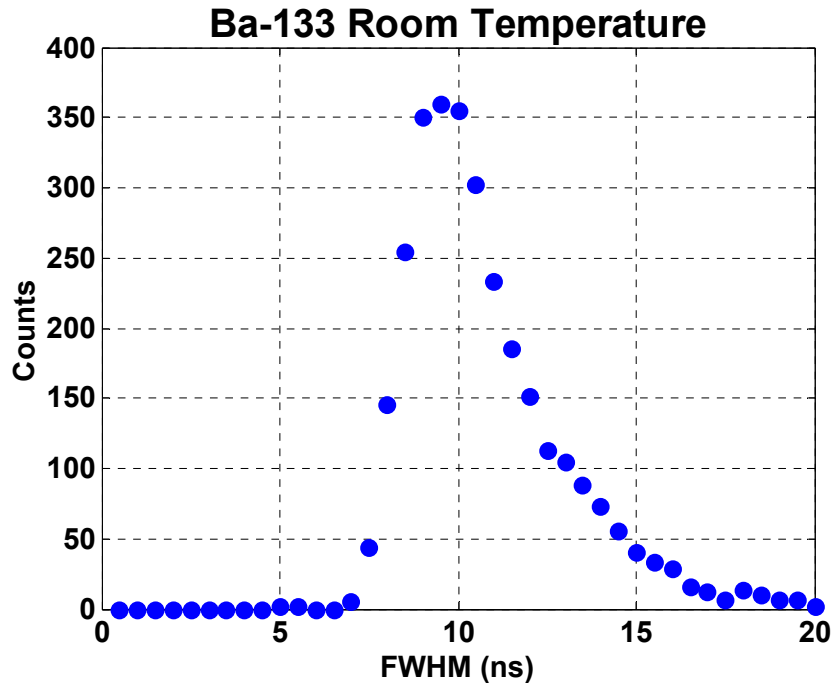
Fall Time Distribution

➤ Faster Fall Time also observed Using Beta Source



Measurement Results (non-irradiated RT)

FWHM Distribution



Diamond?

1. Input current = (charge generated per unit track length) x (saturation velocity). **Silicon**, with more charge but a lower saturation velocity **provides a net 35% more** current for equal track lengths.
2. But diamond's lower capacitance could give it a faster turn-on.
3. Diamond sensors have essentially no leakage currents due to their large band gap.
4. But the radiation hardness of diamond is essentially no better than that of silicon, making further hardening measures necessary. If 3D electrodes are needed for diamonds, the specialized fabrication technology development has to be started and completed.
5. The net result could be a useful but limited advantage given the smaller industrial base for diamond, the greater cost, and other possible difficulties such as ones that might arise from the more than factor of two difference in coefficients of thermal expansion with a diamond pixel sensor and its readout chip as the chips become larger.

NEXT

1. Reduce as far as practicable, the sensor capacitance.
2. Use reduced temperatures to reduce noise and double speeds.
3. Use an amplifier with the lowest possible noise, given the available space, heat removal capabilities, and speed requirements.
4. Use higher electric fields giving drift velocities \approx saturation values.
5. Use trench-electrode sensors.
6. Use waveform recorders if a channel can fit within the area of a pixel. Only the large-amplitude part of the signal is needed. The baseline average can be kept as a single, updated number in storage.
7. Use multiple timing layers of detectors, if allowed by Coulomb scattering, space, and cost considerations – some possibly rotated to help with tracking,
8. Use a weighting factor, as suggested by the time-resolution vs. pulse height results, to favor layers having high signal-to-noise ratios.
9. Considering 6-8 above, use high-resolution position-tracking layers. **The most accurate timing will be done by a system, not by one sensor – readout unit.**

Some Partial Conclusions

- **With the latest 3D results we have seen a decrease in pulse times by 3 orders of magnitude.**
- **There should be possibilities of silicon sensor systems with time resolution well below 100 ps.**
- **The lowest times will use some combination of multiple layers, lower capacitances, higher voltages than the 20V we used, 1/amplitude weighting, lower temperatures, and/or improved electronics.**
- **Improved, fast, compact, wave-form digitizers could help.**
- **We can expect generic electronics certainly will also be improved by industry.**